IMPAIRED AUTONOMIC REGULATION OF THE SINOATRIAL NODE IN DIABETES MELLITUS

by

Pooja S. Krishnaswamy

Submitted in partial fulfilment of the requirements
for the degree of Master of Science

at

Dalhousie University
Halifax, Nova Scotia
July 2014

TABLE OF CONTENTS

LIST OF FIGURES

ABSTRACT

Diabetes mellitus type 1 (T1D) and type 2 (T2D) are frequently associated with a number of cardiovascular complications. Cardiovascular autonomic neuropathy (CAN) is a severe cardiovascular complication in diabetes and results in a progressive decline of proper autonomic regulation of heart rate. CAN is associated with impaired parasympathetic and sympathetic responsiveness of the heart and was originally thought to be solely a consequence of nerve damage. In this study we used both *in vivo* and *ex vivo* techniques to investigate the effects of parasympathetic and sympathetic agonists on the activity of the sinoatrial node (SAN) in diabetic mice. Our measurements show responsiveness of the SAN to sympathetic and parasympathetic agonists is blunted in diabetic mice and that this impairment is reversed by insulin treatment. This work implicates intrinsic alterations in the SAN itself in diabetes. These experiments provide novel insight into the impaired autonomic regulation of the heart in diabetes.

LIST OF ABBREVIATIONS AND SYMBOLS USED

%	Percentage
°C	Degrees Celsius
β-AR	-adrenergic receptor
ACh	Acetylcholine
AP	Action potential
ATP	Adenosine triphosphate
AVN	Atrioventricular node
ANS	Autonomic nervous system
CAN	Cardiovascular autonomic neuropathy
cAMP	Cyclic adenosine monophosphate
CCh	Carbachol
CNS	Central nervous system
cSNRT	Corrected sinus node recovery time
CT	Crista terminalis
CV	Conduction velocity
T1D	Diabetes mellitus type 1
T2D	Diabetes mellitus type 2
DD	Diastolic depolarization
ECG	Electrocardiogram
g	Gram
G_i	Inhibitory G protein
GIRK	G protein inward rectifier potassium channel
GPCR	G protein coupled receptor
G_s	Stimulatory G protein
HCN	Hyperpolarization-activated cyclic-nucleotide gated
HR	Heart rate
HRV	Heart rate variability
Hz	Hertz
$I_{Ca,L}$	L-type calcium current
$I_{Ca,T}$	T-type calcium current

I_f	Hyperpolarization-activated “funny” current
I_{k1}	Inward rectifier potassium current
I_k	Delayed rectifier potassium current
I_{KACh}	Acetylcholine-activated inward rectifier potassium current
I_{Na}	Inward sodium current
I_{NCX}	Na^+-Ca^{2+} exchange current
IP	Intraperitoneal
ISO	Isoproterenol
Kg	Kilogram
L	Litre
LBD	Ligand binding domain
mA	Milliampere
MAP	Mean arterial pressure
MDP	Maximum diastolic potential
mM	Micromolar
mg	Milligram
min	Minute
ml	Millilitre
mm	Millimetre
ms	Millisecond
M	Molar
M2	Muscarinic receptor
nm	Nanometer
nM	Nanomolar
NOD	Non obese diabetic
PI3K	Phosphatidylinositol-4,5-bisphosphate 3-kinase
PKA	Protein kinase A
PSNS	Parasympathetic nervous system
RMP	Resting membrane potential
s	Second

SAN	Sinoatrial node
SNRT	Sinus node recovery time
SNS	Sympathetic nervous system
SPF	Specific pathogen free
SR	Sarcoplasmic reticulum
STZ	Streptozotocin
µg	Microgram
µl	Microlitre
uM	Micromolar

ACKNOWLEDGEMENTS

First and foremost I would like to express my gratitude to my supervisor, Dr. Robert Rose for providing me with this opportunity. I greatly appreciate all of your guidance and support through my research endeavors. Your immense knowledge and passion for cardiovascular science are truly an inspiration. You have helped me to gain so much knowledge in my field, and have also taught me how to think and act critically in many different situations. It has truly been a pleasure to work with you and thank you for such an enriching experience.

I would also like to extend my sincerest thanks to the members of my supervisory committee; Dr. Alex Quinn and Dr. Younes Anini for their encouragement, guidance and support over the course of my research project. You have each taught me so much and without your help my project would not be what it is today.

To my fellow members of the Rose Lab both past and present, thank you for your friendship, encouragement and support both in an out of the lab. You have helped make this experience a truly memorable one and I wish you all the best in your future endeavors. A special thanks to Dr. Rui Hua and Dr. Emmanuel Egom, Kimberly Vella, and Hailey Jansen for your immense assistance with my research project and for your advice throughout this experience.

Finally I would like to express my deepest gratitude to my family and friends for their love and support and for always being there for me throughout the good moments, and especially the tough ones. Mom and Dad, I would not be where I am

today without you. Words cannot express my gratitude for everything you both have done for me.

CHAPTER 1: INTRODUCTION

1.1 Overview

Diabetes mellitus, including both type 1 diabetes (T1D) and type 2 diabetes (T2D), are becoming increasingly prevalent worldwide. It is estimated that over 300 million people worldwide are living with diabetes (Danaei *et al.* 2011). Of that number T1D accounts for about 5-10% of cases, and T2D accounts for about 90% (WHO, 1999). T1D and T2D are characterized by the presence of profound hyperglycemia and irregular metabolism of glucose. T1D is a form of the disease in which the body is unable to manufacture mature insulin due to the destruction of pancreatic islet beta cells; thus, in T1D, there is a complete lack of insulin. T2D, in contrast, is characterized by hyperglycemia in the setting of insulin resistance (i.e. insulin is produced in type 2 diabetics, but is not effective at the tissue level in a normal fashion). Insulin resistance can be due to several factors including insufficient production by the pancreas, loss of responsiveness to insulin at target cells and others. Thus, as a result of environmental factors and possible genetic predispositions the tissues of the body that insulin would normally target to stimulate glucose uptake become resistant to the actions of insulin in the setting of diabetes.

T1D and T2D are closely linked with several cardiovascular complications. In fact, cardiovascular disease is the leading cause of death and morbidity in diabetic patients. One particularly severe, yet often overlooked complication of diabetes is cardiovascular autonomic neuropathy (CAN), which results in an inability of the autonomic nervous system (ANS) to properly regulate heart rate (HR) as well as other aspects of cardiovascular function. Much of the research on CAN implicates nerve

damage as the primary cause of cardiovascular autonomic dysfunction in the diabetic heart. Recent work, on the other hand, suggests that defects in the autonomic regulation of HR may in part be due to alterations within the heart itself, specifically in the pacemaker tissues of the sinoatrial node (SAN). The SAN, which is the primary pacemaker of the heart, determines HR intrinsically based on its rate of spontaneous action potential generation. The sympathetic (SNS) and parasympathetic (PSNS) branches of the autonomic nervous system abundantly innervate the heart, especially at the level of the SAN. Parasympathetic modulation of HR is controlled by the release of acetylcholine (ACh) from the vagus nerve, which binds to muscarinic (M_2) receptors in pacemaker myocytes. Sympathetic modulation is achieved through the action of neurotransmitters released from sympathetic nerve terminals in the SAN, including epinephrine and norepinephrine, which act on ß-adrenergic receptors. Since SAN myocytes are able to spontaneously generate action potentials (AP) and thus initiate electrical conduction in the heart spontaneously, the frequency of AP firing ultimately dictates HR. The parasympathetic and sympathetic branches of the autonomic nervous system have profound effects on heart rate by modulating the frequency of spontaneous action potential firing in the SAN.

Recent work has demonstrated that the heart rate response to a parasympathetic agonist carbachol (CCh) in Akita (type 1) diabetic mice is blunted compared to wildtype littermates; however the specific role of the SAN in this response has not been investigated. This work lead us to investigate heart rate and SAN function in the context of autonomic responsiveness in diabetes. We used the Akita mouse model of type 1 diabetes and the $Lepr^{db/db}$ model of type 2 diabetes to

study the effects of CCh on heart rate and SAN function *in vivo* (using intracardiac programmed stimulation) as well as in isolated atrial preparations (using high-resolution optical mapping). Our hypothesis was that altered parasympathetic responsiveness in diabetes is associated with intrinsic alterations in the SAN and how it responds to parasympathetic agonists. As diabetic patients with CAN also display impaired sympathetic regulation of the heart, we hypothesized that Akita diabetic mice would display impaired responses to isoproterenol (β-adrenergic receptor agonist) within the SAN. This latter hypothesis was tested in isolated atrial preparations using high-resolution optical mapping of the SAN.

1.2 Diabetes mellitus and cardiovascular complications of diabetes.

1.2.1 Type 1 and type 2 diabetes mellitus

Diabetes mellitus is a growing epidemic worldwide (Zimmet *et al.* 2001; Wild *et al*. 2004). It is one of the most common and chronic diseases in almost all countries (Shaw *et al.* 2009). Diabetes mellitus currently affects 380 million people worldwide and its prevalence is predicted to increase by 69% in developing countries, and by 20% in developed countries, by the year 2030. These global estimates clearly demonstrate that diabetes is a growing international health burden (Whiting *et al.* 2011).

Diabetes mellitus is a severe and lifelong condition that affects the body's metabolic processes. Although both T1D and T2D are characterized by elevated blood glucose levels, they differ in their respective pathologies. T1D results from an autoimmune destruction of insulin producing pancreatic beta cells in genetically

susceptible hosts (Gan *et al.* 2012). The immune response is initiated when macrophages and dendritic cells present beta-cell antigens to $CD4^+$ T-cells through the major histocompatibility complex (Atkinson and Maclaren, 1994; Yoon and Jun, 2005). These autoreactive $CD4^+$ T cells become activated through a series of interleukin signaling pathways causing them to secrete cytokines. This activates beta-cell specific cytotoxic $CD8^+$ T cells responsible for beta cell death. Ultimately this results in a complete deficiency of insulin. Clinically, T1D results in prolonged hyperglycemia, polyuria and polydipsia (Gan *et al.* 2012). In the case of T1D, treatment of hyperglycemia is accomplished through the administration of insulin (Pickup and Keen, 2002). The major metabolic actions of this peptide hormone are to decrease blood glucose levels by stimulating glucose uptake in the liver, skeletal muscle and adipose tissue. Exogenous insulin is given to T1D patients in order to regulate glucose metabolism.

T2D differs from T1D in that hyperglycemia results from a resistance of the body's tissues to insulin action. T2D makes up the majority of diabetes cases, and is commonly associated with obesity. The development of type 2 diabetes mellitus is characterized by a progressive deterioration of glucose tolerance over several years (Weyer *et al.* 1999). In T2D the body's tissues become resistant to the actions of insulin. The mechanisms by which insulin resistance develops have been largely disputed, however a large body of work suggests that as adipose tissue expands there are significant increases in free fatty acid release as well as changes in adipokine signaling (Eaton *et al.* 1969; Ong and Kern, 1989; Wahrenberg 1989). Insulin resistance leads to a disruption of normal insulin signaling. Insulin receptor

expression is down regulated and the insulin receptor tyrosine kinase activity is impaired. This leads to a desensitization of second messenger pathways and thus the normal physiological responses to insulin are impaired. T2D is a progressive disorder where insulin resistance leads to chronic hyperglycemia eventually resulting in β cell failure and reduced insulin secretion.

Both T1D and T2D are linked to a number of physiological pathologies. If diabetes is not managed properly it can result in a number of fatal complications. Some of the most detrimental are those that affect the cardiovascular system and diabetes has been deemed an independent risk factor for cardiovascular disease. Diabetes has been associated with impaired autonomic regulation of the heart, which can have severe consequences. This complication will be expanded upon in the section below.

1.2.2 Cardiovascular complications in diabetes: Cardiovascular autonomic neuropathy

It is widely recognized that both T1D and T2D are associated with a number of severe cardiovascular complications. Cardiovascular complications associated with diabetes are a serious concern as they are a major cause of mortality and morbidity in diabetic patients (Vinik and Zeigler, 2007). One particularly harmful yet overlooked complication is cardiovascular autonomic neuropathy (CAN) which results in abnormal autonomic regulation of heart rate. It is thought to affect up to 90% of diabetic patients (Vinik and Ziegler, 2007). Meta analyses of mortality in diabetic patients with and without CAN reflect profoundly higher mortality rates in

diabetic patients living with CAN than in those without (Maser *et al.* 2003; Vinik and Zeigler, 2007). This suggests a strong link between CAN and mortality in diabetes. The presence of CAN in diabetes has been associated with a significantly greater risk of myocardial infarction, ischemia, heart failure and stroke (Ziegler, 1994; Zeigler 2006; Vinik and Ziegler, 2007). Clinically, CAN usually becomes apparent in patients that have had diabetes for several years (Vinik and Ziegler, 2007). This syndrome is generally thought of as late stage complication of diabetes, although the mechanisms that lead to the progression of symptoms are poorly understood.

Some of the clinical presentations of CAN may include reduced heart rate variability (HRV), fixed heart rate, orthostatic hypotension, altered circadian rhythm of heart rate and blood pressure, exercise intolerance, and QTc interval prolongation (Ziegler 1994; Ziegler 2006; Vinik and Ziegler 2007; Karayannis *et al.* 2012). Many of these manifestations are not seen until late stage progression of CAN and heart function is often already critically compromised by the time CAN is diagnosed. Therefore, research on the pathogenesis and molecular basis of heart rate abnormalities associated with CAN are crucial for those affected by diabetes. Diagnosis of CAN usually involves indirect measures of ANS function involving a battery of tests of autonomic regulation of the cardiovascular system (Ewing and Clarke, 1982; Vinik and Ziegler, 2007; Pop-Busui, 2010; Karayannis *et al.* 2012). There is no widely accepted single approach for diagnosis. Several tests have been designed to decipher autonomic damage such as assessment of HRV, orthostatic hypotension, and 24-hour blood pressure profiles. These provide indexes of both parasympathetic and sympathetic function and can be used in clinical settings. Other

methods such as cardiac sympathetic imaging, microneurography, occlusion plethysmography, and baroreflex sensitivity are used more commonly in the research setting (Ewing and Clarke, 1982; Vinik and Ziegler, 2007; Pop-Busui, 2010; Karayannis *et al.* 2012).

CAN encompasses impairments in both sympathetic and parasympathetic branches of the autonomic nervous system. Rawlings *et al.* (2014) has shown that ß-adrenergic signaling of the SNS is impaired in diabetes. Both clinically and experimentally, recent work has shown that sympathetic responsiveness in the heart is altered in diabetes. Luo *et al.* (2013) demonstrated that STZ-treated mice show reduced HR responses to sympathetic stimulation with isoproterenol (ISO). Similarly, parasympathetic responsiveness is also impaired in diabetes as evidenced by the reduced HRV and decreased control of heart rate demonstrated in humans (Javorka *et al.* 2005). Parasympathetic impairment is perhaps greater than sympathetic impairment (Weston and Gill, 1999).

Much of the research on CAN and autonomic dysfunction in diabetes has been done in the context of nerve fiber damage (Vinik and Ziegler, 2007). It has been suggested that hyperglycemia has detrimental effects on neuronal function and survival (Russell *et al.* 1999) such that proper sympathovagal innervation is lost in diabetes. Although it is evident that nerve damage in diabetes has detrimental effects on heart rate, recent work implicates an altered response within the heart itself to autonomic agonists (Park *et al.* 2009; Zhang *et al.* 2014). The autonomic nervous system heavily innervates the heart and modulates heart rate particularly at the level of the SAN, the natural pacemaker of the heart (Mangoni and Nargeot, 2008;

Monfredi *et al.* 2010). Based on this, it is possible that impaired autonomic regulation of heart rate in diabetes may involve altered responses within the SAN . The physiology of the SAN will be discussed further in the next section.

1.3 Heart rate and electrical conduction

In higher organisms the automaticity of the heart is a unique and fundamental physiological phenomenon (Mangoni and Nargeot, 2008). Electrical impulses are spontaneously generated within the SAN of the heart and electrical propagation occurs in a highly ordered fashion to initiate the coordinated contraction of the heart muscle. The spontaneous impulses are initiated by a specialized population of pacemaker cells in the SAN which demonstrate periodical electrical oscillations (Mangoni and Nargeot, 2008). The atrioventricular node (AVN) and the Purkinje fibers of the specialized cardiac conduction system are also able to generate spontaneous action potentials. The leading pacemaker tissue of the SAN region is primarily responsible for the initiation of electrical impulses and the frequency of spontaneous action potential firing determines heart rate *in vivo*. Rates of spontaneous action potential firing in the SAN (and thus heart rate *in vivo*) are modulated by the sympathetic and parasympathetic branches of the autonomic nervous system, which heavily innervates the SAN. Impulse propagation in normal hearts begins in the pacemaker tissues of the SAN.

1.3.1 Sinoatrial node: The pacemaker of the heart

The SAN is located in the intercaval region in the right atrial posterior wall adjacent to the crista terminalis (CT). It is a structurally and physiologically heterogeneous region of the heart (Mangoni and Nargeot, 2008; Monfredi *et al.* 2010). The pacemaker cells of the SAN exhibit a unique action potential property known as the diastolic depolarization (DD), also referred to as the pacemaker potential (Mangoni and Nargeot, 2008; Monfredi *et al.* 2010). This phase spontaneously depolarizes the membrane voltage to the threshold for the next consecutive action potential following repolarization. Electrical activity of pacemaking is ultimately dependent upon the ion channels in the SAN. Expression of ion channels in the SAN differs from the rest of the working myocardium (Monfredi *et al.* 2010). The diastolic depolarization is generated by several ionic currents such as the T- and L-type Ca^{2+} currents ($I_{Ca,T}$ and $I_{Ca,L}$), the inward Na^{+}-Ca^{2+}exchange current (I_{NCX}) which is driven by Ca^{2+} release from the sarcoplasmic reticulum (SR), and the inward hyperpolarization-activated "funny" current (I_f) carried by hyperpolarization-activated cyclic-nucleotide gated (HCN) channels (Mangoni and Nargeot, 2008; Monfredi *et al.* 2010). The lack of I_{k1} in the SAN also accounts for a more depolarized maximum diastolic potential (MDP) in SAN cells compared to the resting membrane potential in cells of the working myocardium (Monfredi *et al.* 2010). In SAN cells an AP is triggered once the resting membrane potential reaches threshold (as in non-automatic cells); however, the rate of depolarization (i.e. action potential upstroke velocity) in SAN cells is slower than in the rest of the working myocardium (Mangoni and Nargeot, 2008; Monfredi *et al.* 2010). This is because

SAN cells have very little sodium current (I_{Na}) compared to myocytes of the working atrial and ventricular myocardium, and it is I_{Na} that is normally responsible for the AP upstroke in these contractile myocytes in the heart. Instead, the depolarization phase of the AP in SAN cells is heavily reliant on $I_{Ca,L}$ (Mangoni and Nargeot, 2008; Monfredi *et al.* 2010). The frequency of AP firing in SAN cells sets the heart rate. SAN activity is heavily modulated by the autonomic nervous system. Both sympathetic and parasympathetic branches can have profound effects on AP firing in the SAN and thus are responsible for eliciting changes in HR.

1.3.2 Autonomic nervous system regulation of heart rate

The autonomic nervous system is a critical regulator of heart rate. It holds two major divisions; the sympathetic nervous system and the parasympathetic nervous system. The SNS acts to increase heart rate while the PSNS acts in the opposite fashion to decrease heart rate (Mangoni and Nargeot, 2008). The adult heart is densely innervated by both SNS and PSNS. The peripheral nerve fibers of the SNS innervate almost all areas of the heart in both the atrial and ventricular myocardium. The positive chronotropic effect of the SNS on the heart is a result of ß-adrenergic receptor (ß-AR) activation. The sympathetic nerve fibers release catecholamines such as epinephrine and norepinephrine which activate ß-ARs coupled to stimulatory heterotrimeric G-proteins (G_s). The α subunit of G_s is responsible for the activation of adenylyl cyclase which in turn catalyzes the conversion of adenosine triphosphate (ATP) into the second messenger cyclic adenosine monophosphate (cAMP) (Mangoni and Nargeot, 2008; Mighiu and Heximer, 2012). Heart rate is increased

when cAMP binds directly to HCN channels in the SAN causing an increase in the slope of the diastolic depolarization (Mangoni and Nargeot, 2008). cAMP also increases heart rate by activating protein kinase A (PKA), which phosphorylates HCN channels, voltage-gated Ca^{2+} channels and ryanodine receptors on the SR. Phosphorylation of these targets increases I_f, $I_{Ca,L}$, SR Ca^{2+} release (the latter leading to an increase in I_{NCX}) respectively (Mangoni and Nargeot, 2008; Mighiu and Heximer, 2012).

Parasympathetic regulation is mediated by the vagus nerve which heavily innervates the SA node, AV node, and the rest of the atrial myocardium (Zipes, 1990). PSNS modulation of heart rate is mediated by M_2 receptor activation. The neurotransmitter acetylcholine (ACh) acts on M_2 receptors coupled to a heterotrimeric inhibitory G protein (G_i). The α subunit of G_i inhibits the activity of adenylyl cyclase leading to a decrease in the production of cAMP. This causes a decrease in I_f, $I_{Ca,L}$ and I_{NCX} in turn reducing the slope of the diastolic depolarization and thus decreasing heart rate (Mangoni and Nargeot, 2008; Mighiu and Heximer, 2012). Interestingly, the ßγ subunit of G_i proteins associated with M_2 receptors activates the ACh sensitive potassium current (I_{kACh}) by binding directly to the channel made up of G protein gated inward rectifier potassium (GIRK) channel subunits (Mangoni and Nargeot, 2008; Mighiu and Heximer, 2012). Activation of I_{kACh} increases repolarizing K^+ current and therefore hyperpolarizes the maximum diastolic potential. Consequently, the time required to reach threshold for firing of a subsequent action potential is prolonged and heart rate is slowed.

1.3.3 Investigation of sinoatrial node function and morphology through optical mapping

The SAN, although comprising a small region of the heart within the right atrium, is an extremely complex and heterogeneous tissue. Studies of the SAN using high-resolution optical mapping have led to important discoveries about cardiac pacemaker activity and the underlying electrophysiological mechanisms responsible for it (Mangoni and Nargeot, 2008; Efimov *et al.* 2010). Optical mapping with voltage sensitive dyes is a powerful and highly effective way to study SAN function (Efimov *et al.* 2004; Efimov *et al.* 2010; Herron *et al.* 2012; Azer *et al.* 2014). This is because it allows for simultaneous recording of changes in activation pattern, electrical conduction and action potential morphology from multicellular preparations.

As mentioned, the SAN is located in the right atrial posterior wall at the junction of the crista terminalis and the superior and inferior vena cava in mammals (Boineau *et al.* 1988; Boyett *et al.* 2000; Dobrzynski *et al.* 2005; Efimov *et al.* 2010). Pacemaker myocytes are distributed throughout the right atrial posterior wall from the superior vena cava to the inferior vena cava (Boineau *et al.* 1988; Boyett *et al.* 2000; Dobrzynski *et al.* 2005; Efimov *et al.* 2010) and changes in heart rate are known to be associated with changes in the region of the SAN that displays the dominant frequency of spontaneous activity (Boineau *et al.* 1988; Fedorov *et al.* 2012). The observation that the leading pacemaker site can shift within the SAN and the idea of a distributed pacemaker complex began with the early fundamental work of Meek and Eyster in 1913 and 1914 who demonstrated that slowing heart rate following vagal

stimulation or by cooling the heart could cause migration of the pacemaker site inferiorly within the SAN (Eyster and Meek, 1913; Meek and Eyster, 1914).

Before the development of high-resolution optical approaches, mapping of electrical conduction in the heart was accomplished using microelectrode techniques. The first systematic mapping of the rabbit SAN using 2 microelectrodes was performed by Sano and Yamagishsi in 1965. They demonstrated that the spread of electrical activation was highly anisotropic. Conduction propagated toward the CT on one side of the SAN and demonstrated a block in conduction in the opposite direction towards the atrial septum. This activation pattern has since been confirmed by several other studies, including through the use of high-resolution optical mapping (Efimov et al 1997; Vinogradova et al 1998; Boyett et al 1999).

Recently, optical mapping of activation patterns in the rabbit SAN has demonstrated that the SAN is both functionally and anatomically insulated from the surrounding atrial myocardium. The SAN in mammals such as rabbits and mice is largely a 2-dimensional structure whereas in larger mammals (dogs, humans, etc) it is a 3-dimensional structure (Bleeker *et al.* 1980; Boineau *et al.* 1988; Efimov *et al.* 2010; Federov *et al.* 2009; Federov *et al.* 2010). This difference led to optical mapping studies of the SAN in canine and human hearts to better understand electrical conduction in the SAN in mammals where it has 3 dimensional structure. One model developed to explain electrical conduction in the SAN proposed discrete SAN exit pathways as a mechanism behind the extremely complex conduction within the SAN. This was known as the Boineau-Schuessler SAN model (Boineau et al 1978; Schuessler, 2003). This essentially showed that electrical impulses from the

SAN demonstrate a slow propagation through the SAN and then transfers to the atria through specialized conduction exit pathways, demonstrated in a canine model (Boineau *et al.* 1978). This hypothesis has been confirmed in studies using canine hearts, which demonstrate that with the exception of numerous sinoatrial exit pathways, the SAN in both canine and human hearts is functionally insulated from the atrial myocardium (Federov *et al.* 2009).

The study of SAN dysfunction and disease has long been limited due to an incomplete understanding of the location of the leading pacemaker and how it shifts within the SAN in different conditions (Glukhov *et al.* 2010). The development of optical mapping techniques has broadened our knowledge of SAN function at a multicellular level and has enabled a more accurate investigation of the shifting phenomenon of the leading pacemaker site (Mackaay *et al.* 1980; Boineau *et al.* 1988; Shibata *et al.* 2001; Federov *et al.* 2010). The leading pacemaker site in the SAN dynamically changes according to various conditions.

Numerous studies have shown that the autonomic nervous system controls heart rate and SAN function in association with changes in initial exit site (Bouman *et al.* 1968; Mackaay *et al.* 1980; Schuessler *et al.* 1986; Kodama *et al.* 1996; Beaulieu *et al.* 1997; Vinogradova *et al.* 1998; Fedorov *et al.* 2006, 2010*a*; Glukhov *et al.* 2010). Pacemaker shift in response to vagal stimulation has been demonstrated in both rabbit and dog. These studies show that activation of the parasympathetic nervous system inhibits SAN function in association with slowing of spontaneous activity and inferior shifts (towards the inferior vena cava) in leading pacemaker site (Vinogradova *et al.* 1998; Fedorov *et al.* 2006; Glukhov *et al.* 2010) following

activation of muscarinic receptors. Conversely, it has also been demonstrated that sympathetic nervous system activation speeds spontaneous activity and shifts the initial exit site in the superior direction in the SAN (Fedorov *et al.* 2010*a*; Glukhov *et al.* 2010). It has been proposed that the preferential superior and inferior shifting is due to the differing properties and sensitivities of superior and inferior sinoatrial node conduction pathways to ACh and ISO. This difference exists as a result of spatial differences in ß-adrenergic and muscarinic receptors (Federov *et al.* 2010).

Much of the early research using optical mapping also demonstrates local conduction velocity (CV) in the SAN is relatively low compared to the rest of the working myocardium, typically under 10 cm/s (Bleeker *et al.* 1980; Verheijck *et al.* 2001; Fedorov *et al.* 2006). This is likely related, at least in part, to poor electrical coupling between cells within the SAN, which is thought to be an essential feature that protects the SAN from the repolarizing influences of the surrounding atrial muscle (Boyett *et al.* 2000). CV is affected by a number of parameters including action potential upstroke velocity and cell to cell communication via gap junctions (Boyett *et al.* 2000; Kleber & Rudy, 2004). Previous studies have demonstrated the presence of gap junctions in the SAN in many animal models as well as humans. Gap junctions in the SAN tend to be smaller and more sparse than those found in atrial muscle (Boyett *et al.* 2000). Each gap junction is made up of clusters of serially linked connexons which provide a passage for small molecules to pass between two cell interiors. Each connexon is comprised of 6 transmembrane proteins called connexins (Severs, 1990). A number of connexins are expressed in the heart including Cx37, Cx40, Cx43, Cx45 and Cx46 (Boyett *et al.* 2000; Verheijck *et al.*

2001). Numerous studies have shown that specific connexins are expressed in a region specific fashion within the heart (van Kempen *et al.* 1991; Oosthoek *et al.* 1993; Davies *et al.* 1994; en Velde *et al.* 1995; Coppen *et al.* 1999; Davies *et al.* 1999). Studies on connexin expression in the SAN demonstrate the presence of Cx40 and Cx45 in pacemaker cells and that the expression of Cx43 (abundant in the working myocardium) is relatively negligible. Channels made up of different connexins have been shown to have unique ionic selectivity, conductance, and permeability (Veenstra *et al.*1992; Veenstra *et al.* 1995; Boyett *et al.* 2000; Verheijck *et al.* 2001). Intercellular coupling patterns in the SAN demonstrate a gradual increase from the center to the peripheral regions and this is important for proper impulse conduction from the SAN to the surrounding atrial muscle (Joyner and van Capelle, 1986; Boyett *et al.* 2000).

Action potential upstroke velocity is another important contributor to overall CV in the SAN (Federov et al 2006; Glukhov *et al.* 2010). Unlike atrial myocytes, upstroke velocity in the SAN, particularly the central SAN, is heavily dependent upon L-type Ca^{2+} current. This results in comparatively low action potential upstroke velocities in SAN myocytes, which is likely a contributing factor to the slow CV typical of the SAN (Kleber & Rudy, 2004).

Parasympathetic effects on CV in the SAN are thought to be largely due vagal activation of I_{kACh} and inhibition of $I_{Ca,L}$ current in SAN myoctyes. This depressant effect on $I_{Ca,L}$ may affect AP upstroke velocity and amplitude via the inhibition of AC activity causing a decrease in cAMP production, and thus dephosphorylation of Ca^{2+} channels. Activation of I_{kACh} causes hyperpolarization, increasing cycle length and

shortening the SAN AP (Kodama *et al.* 1996). Sympathetic effects are elicited through the binding of sympathetic agonists to ß-adrenergic receptors.

1.3.4 Investigation of sinoatrial node function using ECG and programmed electrical stimulation

Rhythmic and synchronized contraction of the atria and ventricles is imperative for maintenance of sufficient cardiac output. This is achieved through the actions of a specialized electrical conduction system in the heart that begins with the spontaneous activity of the SAN (Boyett, 2009). Abnormalities in the initiation and/or conduction of electrical impulses throughout the heart can lead to the generation of cardiac arrhythmias; therefore recording the electrical activity of the heart *in vivo* is an invaluable research and clinical tool. The technique intracardiac programmed stimulation has immensely increased the understanding of cardiac function (Tonkin *et al.* 1980). It has played a key role in the recognition of SAN disorders as well as AVN disorders and those concerning the rest of the ventricular condition system.

Sinoatrial node function is assessed *in vivo* via intracardiac programmed electrical stimulation and the measurement of sinus node recovery time (SNRT). SNRT is measured after a period of overdrive pacing given at a rate faster than the dominant pacemaker (Narula *et al.* 1972; Tonkin *et al.* 1980). It is essentially a measure of the time required for the SAN to resume initiation of heart beats following the cessation of atrial pacing (Chadda *et al.* 1975). The true measure is known as the corrected sinus node recovery time (cSNRT) in which the original SNRT is adjusted

by accounting for the pre-stimulus heart rate. This methodology is widely used and recognized both experimentally and clinically as a measure of SAN function (Narula *et al.* 1972; Chadda *et al.* 1975; Tonkin *et al.* 1980). Studies indicate cSNRT is a reproducible measure with minimal variability particularly at high paced rates in both normal and dysfunctional nodes (Narula *et al.* 1972; Chadda *et al.* 1975). The measurement is significantly affected by induced changes in vagal and sympathetic tone as well as a range of injury or disease states. Thus changes in cSNRT brought on by autonomic interventions are of potential clinical significance in the setting of disease and dysfunction in autonomic regulation of the SAN (Chadda *et al.* 1975).

1.4 Animal models of type 1 and type 2 diabetes mellitus

Rodent models of diabetes are frequently used in research, and their use over the past 150 years has been instrumental in the field of diabetes and insulin treatment development (Thayer *et al.* 2010). The use of various mouse models of diabetes in research is frequently debated as each model possesses particular strengths and weaknesses. Nevertheless, mouse models of diabetes have enabled the discovery of fundamental information (Hall and Cooke, 2011). The rationale for the specific models used in the present study will be discussed in further detail below.

1.4.1 Akita mouse model of type 1 diabetes mellitus

In the present study cardiovascular function in insulin-dependent diabetes was studied using the Akita mouse. The Akita mouse model of type 1 diabetes is a transgenic model containing a mutation in the insulin 2 (*Ins2*) gene. The resulting

amino acid substitution replaces a cysteine with tyrosine at the seventh amino acid of the A chain of the insulin 2 gene product, blocking the formation of an essential disulfide bond between the A and B chains of the mature protein (Wang *et al.*1999; Izumi *et al.* 2003; Oyadomari *et al.* 2005). The mutation results in a conformational change in the protein, leading to its accumulation in the endoplasmic reticulum of pancreatic β cells, which triggers the unfolded protein response and causes a significant depletion of islet ß cells as well as ß cell dysfunction and thus very little to no mature insulin is produced (Wang *et al.* 1999; Lu *et al.* 2007). This model is ideal for the study of type 1 diabetes as it mimics the clinical features of human maturity-onset diabetes (Kayo and Koizumi 1998). Akita mice are also known to develop neuropathies similar to humans, which is critical for my project (Hsueh *et al.* 2007). The use of this model is preferred over other common type 1 diabetic mouse models such as the chemically induced streptozotocin (STZ) model and the spontaneous autoimmune non-obese diabetic (NOD) model. The STZ model presents a disadvantage in that STZ has been shown to be toxic to a number of organs in the body and has possible unfavourable side effects such as changing P450 isoenzymes in the liver, kidneys, lungs, intestines, and brain (Lee *et al.* 2010; King, 2012). The NOD mouse is an accurate representation of the true autoimmune component of diabetes seen in humans (Yoon and Jun, 2001), however, a challenge with NOD mice is the development of diabetes is negatively associated with microbial exposure, as well as the gender differences and unpredictability of the disease onset require the mice to kept in specific pathogen free (SPF) conditions (King, 2012).

1.4.2 db/db obese mouse model of type 2 diabetes

As type 2 diabetes is closely linked to obesity many of the current mouse models of type 2 diabetes are obese. Obesity can be induced by high fat feeding or by genetic manipulation. The present study uses the $Lepr^{db/db}$ mouse model, which contains an autosomal recessive mutation in the leptin receptor (Hummel *et al.* 1966; Chen *et al.* 1996). These animals become obese, hyperinsulinemic and hyperglycemic at about 4 weeks of age. The db/db mouse is an advantageous model in the study of type 2 diabetes as it has served as a common rodent model of obesity and diabetes studies for over 40 years and is well characterized (Belke and Severson, 2012). Db/db mice commonly display a more consistent and uniform phenotype compared to other models such as diet induced diabetes. Many features of the diabetic phenotype in db/db mice are similar to humans such as the age-dependent progression of the disease with early onset of insulin resistance, as well as a defect in insulin secretion that leads to profound hyperglycemia. Many other models of type 2 diabetes exist but for the purposes of the present study it was important to use a well characterized model in which the physiological progression of the disease is well characterized and the cardiovascular effects specifically could be elucidated without unknown confounding side effects.

1.5 Impaired responsiveness of the SAN to parasympathetic and sympathetic stimulation in diabetes

The inability of the nervous system to properly regulate heart rate in diabetes has been poorly understood. Until recently, the dysfunction in sympathetic and

parasympathetic control of the heart in diabetes has been attributed to nerve damage and death of the fibers which innervate the heart (i.e. neuropathy). Though this may encompass some of the problem, recent work suggests that the impairment in autonomic responsiveness in diabetes may be associated with intrinsic alterations within the heart itself. Park *et al.* (2009) demonstrated that parasympathetic regulation of HR is impaired in the Akita mouse model of type 1 diabetes. Specifically, the ability of the parasympathetic nervous system agonist CCh to reduce HR is profoundly impaired in Akita mice compared to wildtype littermates. In another study reduced heart rates were seen in diabetic mice in the absence of any changes in structural properties assessed by echocardiography, pointing to a defect in SAN function in the context of diabetes (Luo *et al.* 2013). They also demonstrated impaired heart rate responses in the presence of ISO (a sympathetic agonist). These findings are consistent with known defects in cardiac pacemaker and autonomic dysfunction in diabetic patients. Taken together these data implicate intrinsic alterations in SAN function and its responsiveness to autonomic agonists; however, no direct mechanistic studies of autonomic regulation of the SAN in diabetes have been performed.

1.6 Objectives

T1D and T2D can lead to a number of severe cardiac complications. Previously it has been demonstrated that Akita mice display abnormal heart rate responses to parasympathetic nervous system agonists (Park *et al.* 2009; Zhang *et al.*

2014), however, direct measures of SAN function during parasympathetic activation have not been performed.

To begin the present study we aimed to characterize the presence of altered parasympathetic responsiveness in the SAN of Akita diabetic mice. We investigated heart rate and SAN function in response to a cholinergic agonist CCh *in vivo*. In accordance with previous studies (Park *et al.* 2009; Zhang *et al.* 2014) we hypothesized that Akita diabetic mice would demonstrate impaired heart rate responses as well as altered SAN responsiveness to CCh in comparison to wildtype littermates.

It is known that a critical mechanism by which CCh inhibits SAN activity is by slowing electrical conduction within the SAN (Federov *et al.* 2006, Glukhov *et al.* 2010). In accordance with this we investigated activation patterns in the SAN in response to CCh in Akita diabetic mice. We hypothesized that the effects of CCh on electrical conduction in the SAN would be impaired in Akita diabetic mice compared to wildtype littermates.

To characterize the altered parasympathetic responsiveness in a model of type 2 diabetes we used the db/db mouse model. Similar to the previous objectives we investigated heart rate and SAN function in response to CCh *in vivo* and using high-resolution optical mapping. We hypothesized that db/db diabetic mice would show impaired responses to parasympathetic agonist similar to Akita (type 1) diabetic mice.

Finally, to begin looking at the possible impairment in sympathetic responsiveness of the SAN, I performed high-resolution optical mapping experiments to investigate SAN activation and conduction patterns in Akita diabetic mice in

response to ISO. This was done to test the hypothesis that sympathetic responsiveness of the SAN would also be impaired in Akita diabetic mice compared to wildtype littermates.

CHAPTER 2: MATERIALS AND METHODS

2.1 Experimental Animals

2.1.1 Ins2^{Akita} Mice

All mice used to study altered parasympathetic and sympathetic responsiveness in type 1 diabetes were male littermate wildtype and C57BL/6 *Ins2*^{Akita} diabetic mice between the ages of 16-20 weeks. Mice were originally obtained from the Jackson Laboratory (strain C57BL/6-*Ins2*^{Akita}/J) and then bred and housed at a maximum of five per cage in the Carleton Animal Care Facility at Dalhousie University. All mice were maintained on a 12-hour light/dark cycle and were fed standard rodent chow which was provided *ad libitum.* All experimental protocols were in accordance with the regulations of The Canadian Council on Animal Care and were approved by Dalhousie University. *Ins2*^{Akita} mice possess a point mutation of the insulin-2 (Ins2) gene whose product replaces a cysteine residue that is engaged in the formation of an intramolecular disulfide bond (Kayo and Koizumi, 1998). This results in the destruction of pancreatic beta cells and thus produces the type 1 diabetic phenotype. Mice heterozygous for the spontaneous mutation are viable and characterized by hyperglycemia, hypoinsulinemia, polydipsia, and polyuria beginning around 3-4 weeks of age and stabilizing at about 12 weeks of age (Fujta *et al.* 2001). Male wildtype and heterozygotes mice were used in this study.

Monitoring of the diabetic phenotype was done using Keto-Diastix (Bayer) for urinalysis to discern between wildtype and Akita mice at 4 weeks of age. At the time

of experiments a standard blood glucose meter and lancet strips were used to obtain blood glucose levels in wildtype and Akita mice.

In some experiments Akita mice were treated with insulin (or placebo) for 4 weeks beginning at 12 weeks of age. This was done by implanting insulin pellets (or placebo) (LinShin Canada) subcutaneously. These pellets release 0.1 units of insulin/day. The number of implants given to each mouse was based on body weight(as determined by the manufacturer) whereby 2 pellets were implanted for the first 20 g of body weight and then 1 pellet for every 5 g thereafter. Mice were anesthetized by isoflurane inhalation (3%) and pellets were implanted via a small puncture in the skin according to the manufacturer's instructions. Blood glucose was monitored in these animals before pellet implantation and then every 3 days for 4 weeks after treatment began until the animals were used experimentally at 16 weeks of age.

2.1.2 db/db Mice

To investigate altered parasympathetic responsiveness in type 2 diabetes we used an obese mouse model of diabetes, the db/db mouse (Jackson Laboratories) (strain BKS.Cg-*Dock7m* +/+ *Lepr*^{db}/J). Male db/db mice and control C57BL/6 mice were used between the ages 16-20 weeks. Mice were housed at a maximum of five per cage in the Carleton Animal Care Facility at Dalhousie University. All mice were maintained on a 12-hour light/dark cycle and were fed standard rodent chow which was provided *ad libitum.* All experimental protocols were in accordance with the regulations of The Canadian Council on Animal Care and were approved by

Dalhousie University. Db/db mice are characterized by a point mutation in the gene for the leptin receptor, which causes a deficiency in receptor activity (Chen *et al.* 1996; Lee *et al.* 1996). Db/db mice homozygous for the mutation become obese at approximately 3-4 weeks of age and blood sugar becomes elevated at 6-8 weeks of age (Garris and Garris, 2003; Garris, 2004; Greer *et al.* 2006).

2.2 Pharmacological Compounds

Experiments designed to study parasympathetic responsiveness of the heart were performed using carbamylcholine chloride (carbachol; CCh). This compound acts on muscarinic (M_2) receptors and mimics the effects of acetylcholine (Lei *et al.* 1999). For *in vivo* work CCh stock solution (0.01 mg/ml) was made in double distilled water and was injected intraperitoneally at a dose of 0.1 mg/kg. In optical mapping experiments CCh stock solution (10 mM) was made in double distilled water and was superfused onto atrial preparations at a final concentration of 0.1 μM.

To investigate sympathetic responsiveness experiments were performed using the β-adrenergic receptor agonist isoproterenol (ISO). In optical mapping experiments ISO stock solution (1×10^{-3} M) stock was made in double distilled water and was superfused onto atrial preparations at a final concentration of 10 nM.

2.3 Experimental Approaches

2.3.1 Surface and Intracardiac ECG Recordings

Mice were anesthetized (2-2.5% isoflurane inhalation in 0.9 L/min O_2) and placed on a heating pad to maintain normal body temperature (37 ± 1 °C), which was

monitored using a rectal thermometer. Surface ECGs were recorded using three 30 gauge subdermal needle electrodes (Grass Technologies) inserted in a lead II position. For intracardiac ECGs a 1.1 French octapolar electrode electrophysiology catheter (Transonic Scisense Inc, London ON) was inserted into the right jugular vein of anesthetized mice (3% isoflurane in 1.0 L/min O_2) and advanced through the right atrium into the right ventricle via the tricuspid valve. All surface and intracardiac ECG signals were recorded, amplified and filtered between 0.3 Hz and 300 Hz using a Gould ACQ-7700 amplifier and the Ponemah Physiology Platform software (version 4.60, Data Sciences International).

SNRT, a clinical measure of SAN function (Narula *et al.* 1972; Chadda *et al.* 1975; Tonkin *et al.* 1980; Gomez *et al.* 1984), was measured by delivering a 12 stimulus drive train at a cycle length of 100 ms in the right atrium. SNRT is defined as the time between the last stimulus in the drive train and the onset of the first spontaneous sinus beat (designated by the start of the P wave). To correct for heart rate, corrected SNRT (cSNRT) was calculated by subtracting the prestimulus R-R interval from the measured SNRT (cSNRT= SNRT-RR; Figure 2.1).

2.3.2 High-resolution Optical Mapping

Optical mapping studies were performed using an isolated atrial preparation, which enables the visualization of electrical propagations in the SAN within the right atrial posterior wall (Fig. 2.2). Isolated atrial preparations were prepared by administering a 0.2 mL intraperitoneal inection of heparin (1000 IU ml^{-1}) to mice to prevent blood clotting. Mice were then anaesthetized by isoflurane inhalation and

cervically dislocated. Hearts were excised and transferred to a Krebs solution (35°C) containing (in mM): 118 NaCl, 4.7 KCl, 1.2 KH_2PO_4, 12.2 $MgSO_4$, 1 $CaCl_2$, 25 $NaHCO_3$ and 11 glucose. This Krebs solution was bubbled with 95% O_2/5% CO_2 to maintain a pH of 7.4. Atria were dissected away from the ventricles and pinned in a dish with the endocardial surface

Figure 2.1: Assessment of sinoatrial node function *in vivo* by determination of sinoatrial node recovery time (SNRT). An octapolar catheter was used to deliver 12 stimulated beats to the atria and the interval between the last stimulated beat and the P wave of the first spontaneous sinus beat was measured. In this example, it took 144 ms for the first P wave to appear after the last stimulated beat. SNRT is corrected by subtracting the intrinsic RR interval during normal sinus rhythm (108 ms in the above example) for a corrected SNRT (cSNRT) of 36 ms.

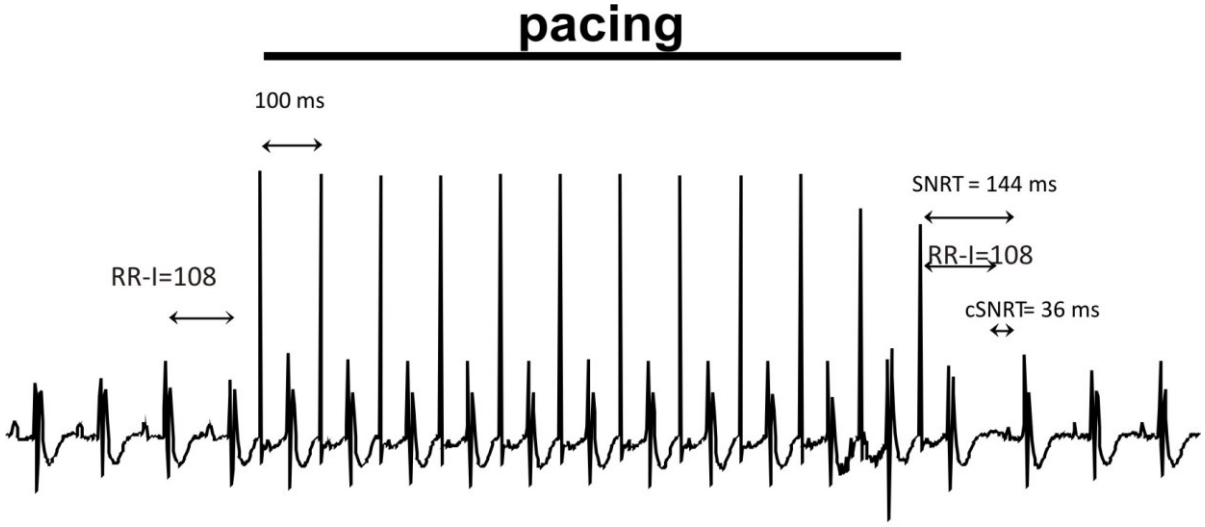

Figure 2.1

facing upward. The superior and inferior vena cavae were cut open in order to visualize the SAN region located in the intercaval region, adjacent to the crista terminalis (Figure 2.2). The preparations were continuously superfused with Krebs solution (35°C) and bubbled with 95% O_2/5% CO_2. The preparations were treated with the voltage sensitive dye di-4-ANEPPS (10 μM) for 15 minutes and blebbistatin (10 μM) was added to suppress contractile activity. Most experiments were performed in sinus rhythm so that the cycle length (i.e. heart rate) of the atrial preparation was free to change. In a subset of studies we used a unipolar pacing electrode to pace atrial preparations at a fixed cycle length of 120 ms to study effects of CCh on changes in electrical conduction independently of changes in heart rate. When used, the pacing electrode was placed near the opening of the superior vena cava.

Atrial preparations were illuminated with light at a wavelength of 520–570 nm using an EXFO X-cite fluorescent light source (Lumen Dynamics, Mississauga, Ontario, Canada). Emitted fluorescent light (590–640 nm) was captured using a high speed EMCCD camera (Evolve 128, Photometrics, Tucson, AZ, USA). This camera contains a 128 × 128 pixel array and, in our experimental setup, each pixel measured 77 × 77 μm, which results in a maximum field of view on the atrial preparation of approximately 10 × 10 mm. Magnification was constant in all experiments and no pixel binning was used; thus, this pixel size remained constant in all measurements. Data were captured at a frame rate of approximately 1000 frames s^{-1} using Metamorph software (Molecular Devices, Sunnyvale, CA, USA). All data were analysed using custom software written in Matlab. Analyses included pseudocolour electrical activation maps and isochronal contour plots, which were generated from measurements of activation time at individual pixels. Local

Figure 2.2: Mouse atrial preparation used for optical mapping experiments.

The preparation is orientated so that the right atrium is on the right side of the image. RAA, right atrial appendage; CT, crista terminalis; SVC, opening of superior vena cava; IVC, opening of inferior vena cava; The sinoatrial node (SAN) is located in the intercaval region adjacent to the CT (dotted line). Scale bar = 2 mm

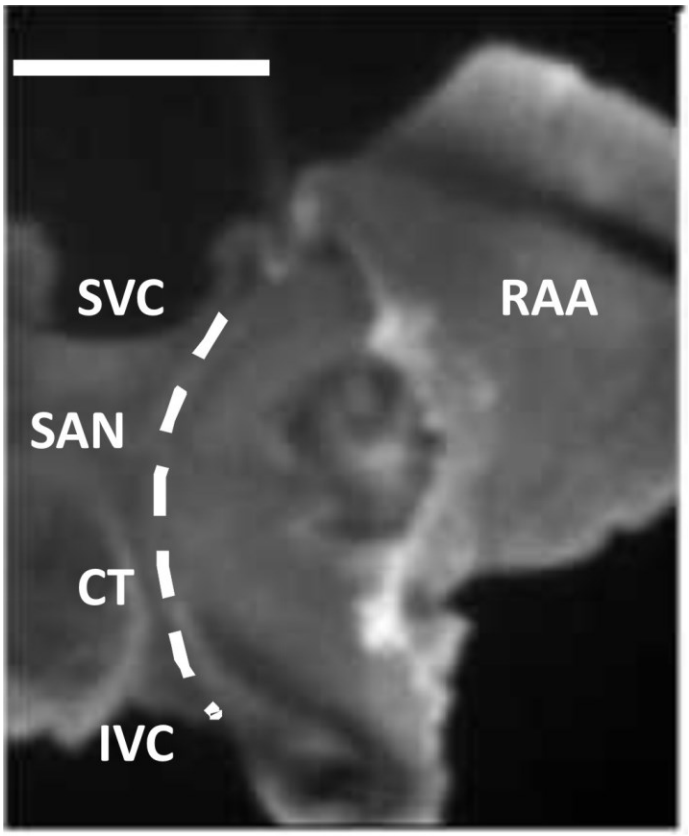

Figure 2.2

conduction velocity (CV) was quantified specifically in the SAN at the site of initial electrical breakthrough, using a previously validated method (Morley *et al.* 1999; Nygren *et al.* 2004; Azer *et al.* 2014). Briefly, activation times at each pixel from a 7 × 7 pixel array were determined and fit to a plane using the least squares fit method. The direction on this plane that is increasing the fastest represents the direction that is perpendicular to the wavefront of electrical propagation and the maximal slope represents the inverse of the speed of conduction in that direction. Thus, using this method, we computed maximum local CV vectors in the atrial region of interest.

2.4 Statistical Analysis

Statistical analyses were performed using SigmaPlot (version 11.0; Systat Software, Inc., San Jose, CA). Paired Student`s *t*-tests were used for comparison of single parameter means. Differences between means were also evaluated by a two-way analysis of variance (ANOVA) followed by Tukey's post-hoc test. All summary data are presented as mean ± SEM. In all cases, $P<0.05$ was considered statistically significant.

CHAPTER 3: RESULTS

3.1 Body mass and Blood glucose levels in Akita diabetic mice

To first confirm the presence of hyperglycemia in the Akita mouse, blood glucose levels were measured in both wildtype and Akita animals. Body mass was quantified in these animals to confirm the non-obese diabetic model. Consistent with prior studies body mass was decreased in Akita diabetic animals (Bugger *et al.* 2008) compared to wildtype (24.8 ± 0.4 g in Akita vs. 31.8 ± 1.0 g in wildtype, $P<0.05$) (Figure 3.1A). Figure 3.1B demonstrates that blood glucose levels were markedly increased in Akita diabetic animals compared to wildtype controls (33.5 ± 2.2 mmol/L in Akita vs. 7.5 ± 0.4 mmol/L in wildtype, $P<0.05$) (Figure 3.1B).

3.2 Effects of CCh on heart rate and sinus node function in Akita diabetic mice *in vivo*

In the first set of experiments, the parasympathetic regulation of the SAN was studied by measuring the effects of CCh (0.1 mg/kg, IP injection) on heart rate and cSNRT. Representative examples of these measurements are illustrated in Figure 3.2. Summary data in Figure 3.3A demonstrates heart rate was reduced after CCh injection in both wildtype (545.7 ± 13.0 beats/min at baseline vs. 384.2 ± 15.8 beats/min after CCh, $P<0.05$) and Akita (485 ± 8.5 beats/min at baseline vs. 428.1 ± 13.2 beats/min after CCh, $P<0.05$) animals. The magnitude of the reduction in heart rate elicited by CCh was smaller in Akita diabetic mice compared to wildtypes (161.4 ± 15.5 beats/min in wildtype vs. 56.8 ± 7.8 beats/min in Akita, $P<0.05$) (Figure 3.3B). In conjunction with the

Figure 3.1: Body mass and blood glucose measurements in wildtype and Akita diabetic mice. A. Summary data illustrating the body mass of wildtype and Akita diabetic animals at 16 weeks of age. n=5 *P<0.05 vs. wildtype by Student's *t*-test. B. Summary data illustrates blood glucose levels for wildtype and Akita diabetic animals at 16 weeks of age. n=5 *P<0.05 vs. wildtype by Student's *t*-test.

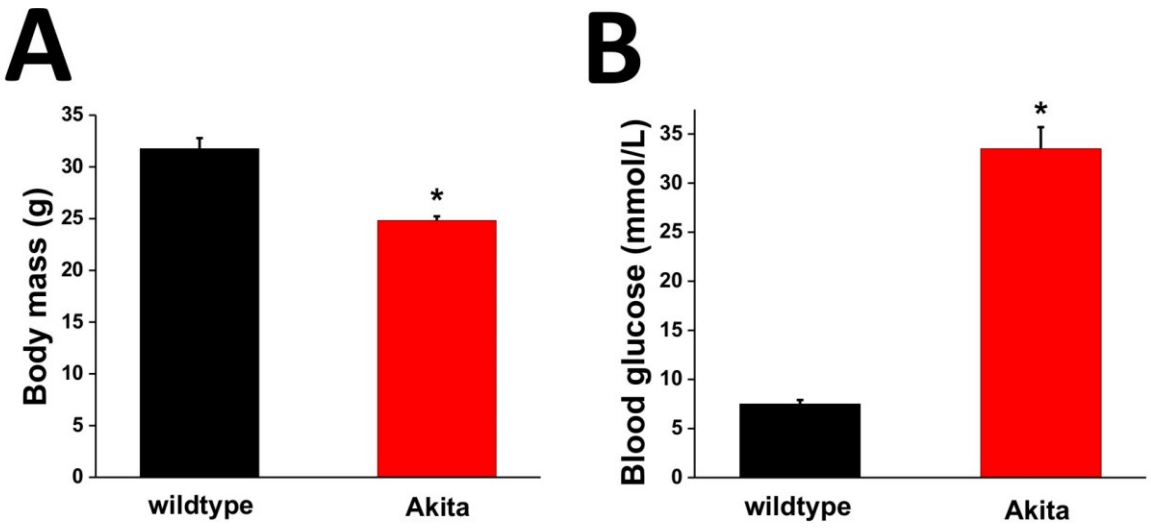
A
Body mass (g)
35
30
25
20
15
10
5
0
*
wildtype
Akita
B
Blood glucose (mmol/L)
35
30
25
20
15
10
5
0
*
wildtype
Akita

Figure 3.1

Figure 3.2: Effect of carbachol (CCh) on sinoatrial node recovery time (SNRT) in anesthetized wildtype and Akita mice. A. Representative ECG recordings illustrating assessment of SNRT under baseline conditions and after intraperitoneal (IP) injection of CCh (0.1 mg/kg) in anesthetized wildtype mice. SNRT is measured by pacing the heart at a cycle length of 100 ms and then assessing the time to the first spontaneous P wave. This SNRT is then corrected for heart rate (HR) by subtracting the R-R interval before pacing to yield the corrected SNRT (cSNRT). B. Representative ECG recordings illustrating the assessment of SNRT under baseline conditions and after IP injection of CCh (0.1 mg/kg) in Akita diabetic mice. Arrows indicate the first spontaneous P wave after pacing. SNRT and cSNRT values are shown for each representative recording.

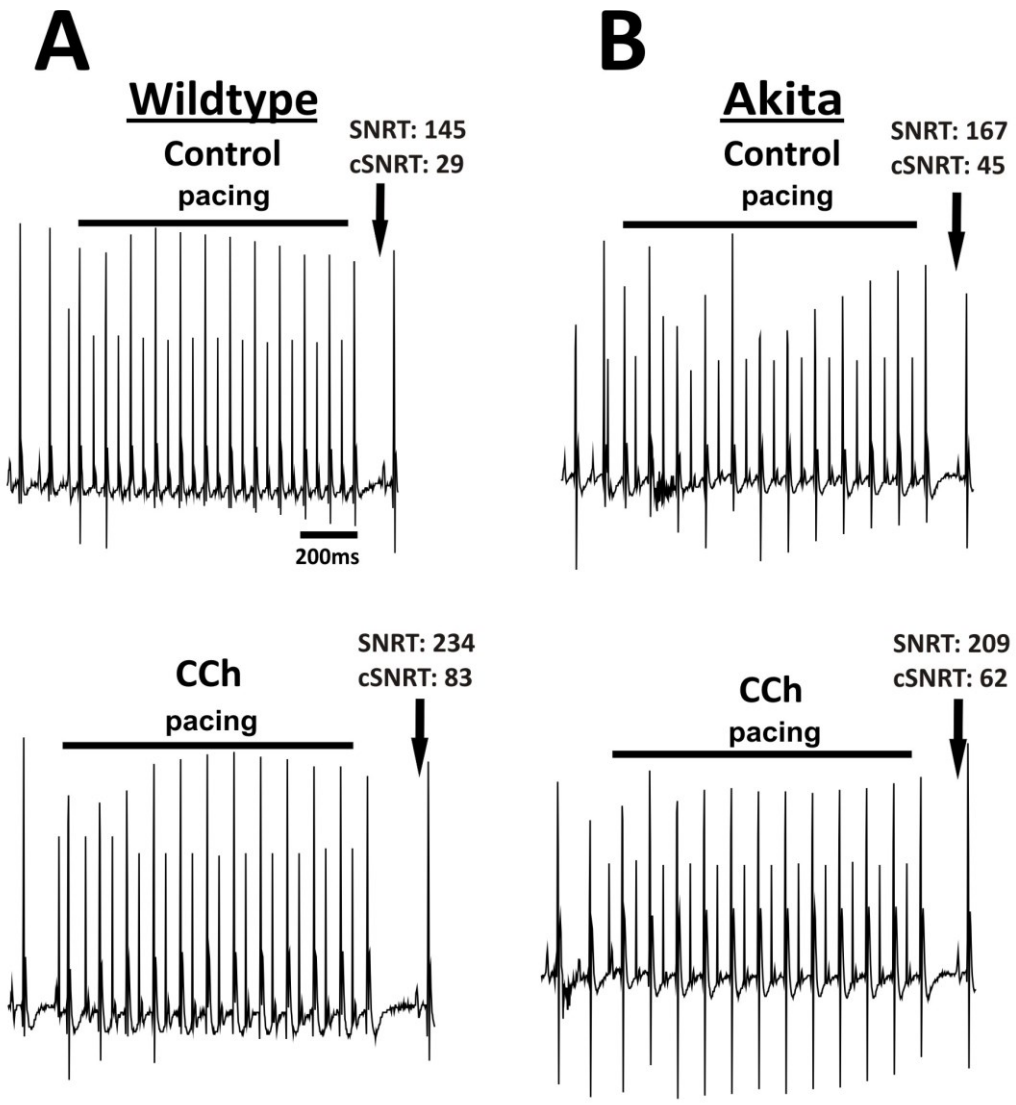
A
Wildtype
Control
pacing
SNRT: 145
cSNRT: 29
200ms
CCh
pacing
SNRT: 234
cSNRT: 83
B
Akita
Control
pacing
SNRT: 167
cSNRT: 45
CCh
pacing
SNRT: 209
cSNRT: 62

Figure 3.2

Figure 3.3: Effects of carbachol on heart rate and sinoatrial node function in wildtype and Akita diabetic mice *in vivo.* A. Summary data illustrating the effects of CCh (0.1 mg/kg IP) on HR in anesthetized wildtype (n=9) and Akita (n=10) mice. *P<0.05 vs. baseline; ^{+}P<0.05 vs. wildtype. Data analyzed by two way ANOVA with Tukey's posthoc test. B. Summary data illustrating the magnitude of the reduction in HR elicited by CCh in wildtype and Akita mice. *P<0.05 vs. wildtype by Student's t-test. C. Summary data illustrating the effects of CCh (0.1 mg/kg IP) on cSNRT in anesthetized wildtype (n=9) and Akita (n=10) mice. *P<0.05 vs. baseline; ^{+}P<0.05 vs. wildtype. Data analyzed by two way ANOVA with Tukey's posthoc test. D. Summary data illustrating the magnitude of the increase in cSNRT elicited by CCh in wildtype and Akita mice. *P<0.05 vs. wildtype by Student's t-test.

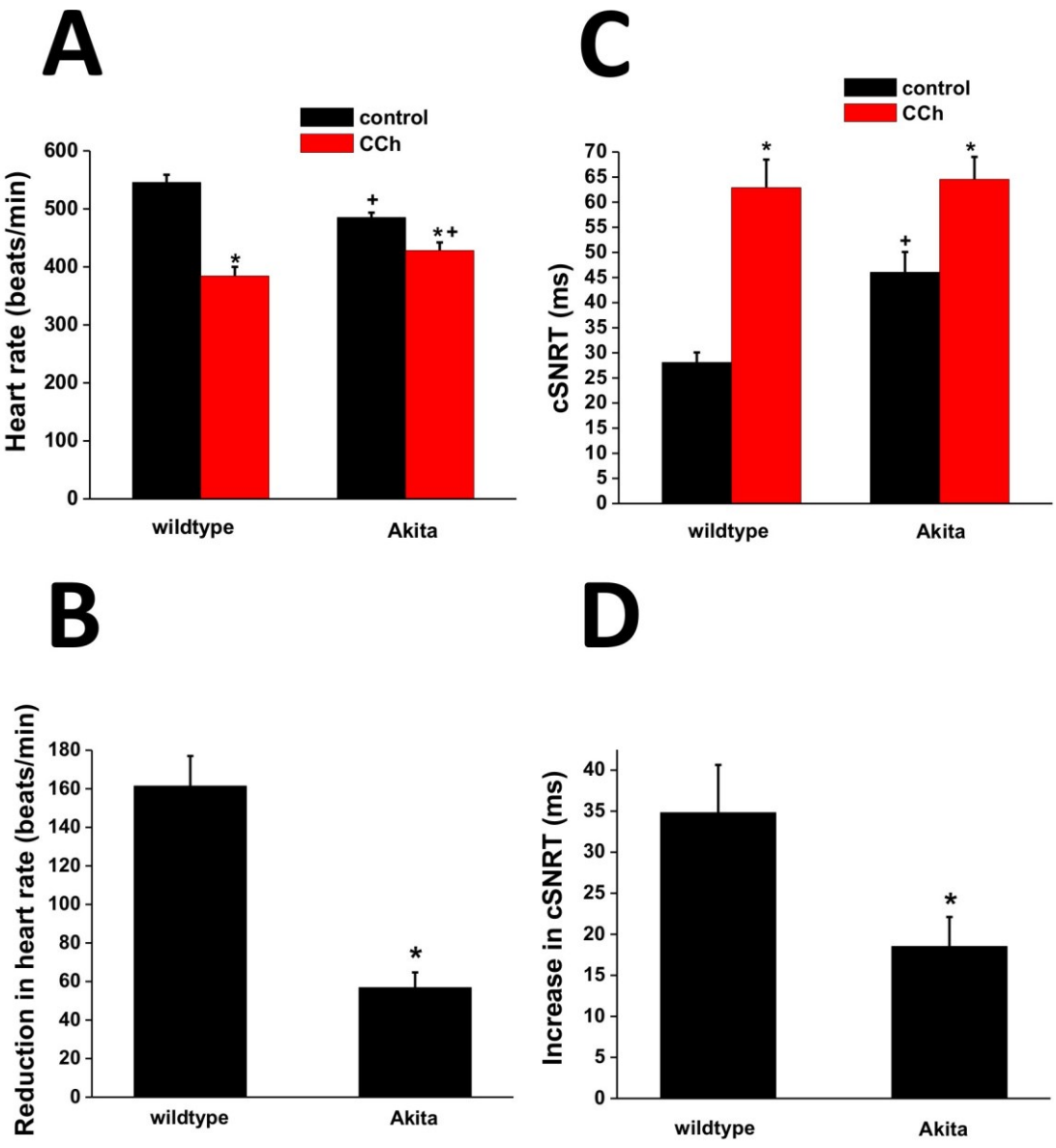
A
control
CCh
Heart rate (beats/min)
600
500
400
300
200
100
0
*
+
*+
wildtype
Akita
C
control
CCh
cSNRT (ms)
70
65
60
55
50
45
40
35
30
25
20
15
10
5
0
*
+
*
wildtype
Akita
B
Reduction in heart rate (beats/min)
180
160
140
120
100
80
60
40
20
0
*
wildtype
Akita
D
Increase in cSNRT (ms)
40
35
30
25
20
15
10
5
0
*
wildtype
Akita

Figure 3.3

reduction in HR figures 3.2 and 3.3 demonstrate that after CCh injection, cSNRT was increased in both wildtype (28.1 ± 1.9 ms at baseline vs. 54.8 ± 7.3 ms after CCh, $P<0.05$) and Akita (46.0 ± 4.0 ms at baseline vs. 62.7 ± 4.7 ms after CCh, $P<0.05$) (Figure 3.3C) mice compared to control conditions; however, the magnitude of the increase in cSNRT elicited by CCh was significantly smaller in Akita diabetic mice compared to wildtype (16.7 ± 4.4 ms in Akita vs. 26.7 ± 7.9 ms in wildtype, $P<0.05$) (Figure 3.3D). Together, these experiments demonstrate that parasympathetic modulation of HR and SAN function is impaired in Akita diabetic mice.

3.3 Effects of CCh on patterns of electrical conduction in the sinoatrial node in Akita diabetic mice.

To begin to understand the mechanisms responsible for altered responses to parasympathetic agonists in the diabetic heart, the effects of CCh on patterns of electrical conduction in SAN were studied using high-resolution optical mapping. These experiments were performed using an isolated atrial preparation (Fig. 2.2) in which we can accurately study electrical propagation in the SAN within the right atrial posterior wall, as we have described previously (Azer *et al.* 2014)

Figure 3.4 demonstrates that application of CCh (0.1 μM) slowed electrical conduction in the right atrial posterior wall in wildtype and Akita mice (note the increase in number of contour lines and decrease in spacing between successive contour lines). The site of initial electrical breakthrough in the SAN was located in the right atrial posterior wall adjacent to the crista terminalis and is referred to as the 'initial exit site' (Federov *et al.* 2012). This is because of the three-dimensional nature of electrical

Figure 3.4: Effects of carbachol on patterns of electrical conduction in the sinoatrial node and right atrial posterior wall in wildtype and Akita diabetic mice. A. Representative colour maps showing activation patterns in control conditions and after application of CCh (0.1 μM) in wildtype and Akita diabetic mice. In these figures the right atrial appendage is on the right side of the image. Red colour indicates earliest activation time (ms) in the SAN within the right atrial posterior wall. Time interval between adjacent isochrones is 1 ms. Scale bars are 2 mm.

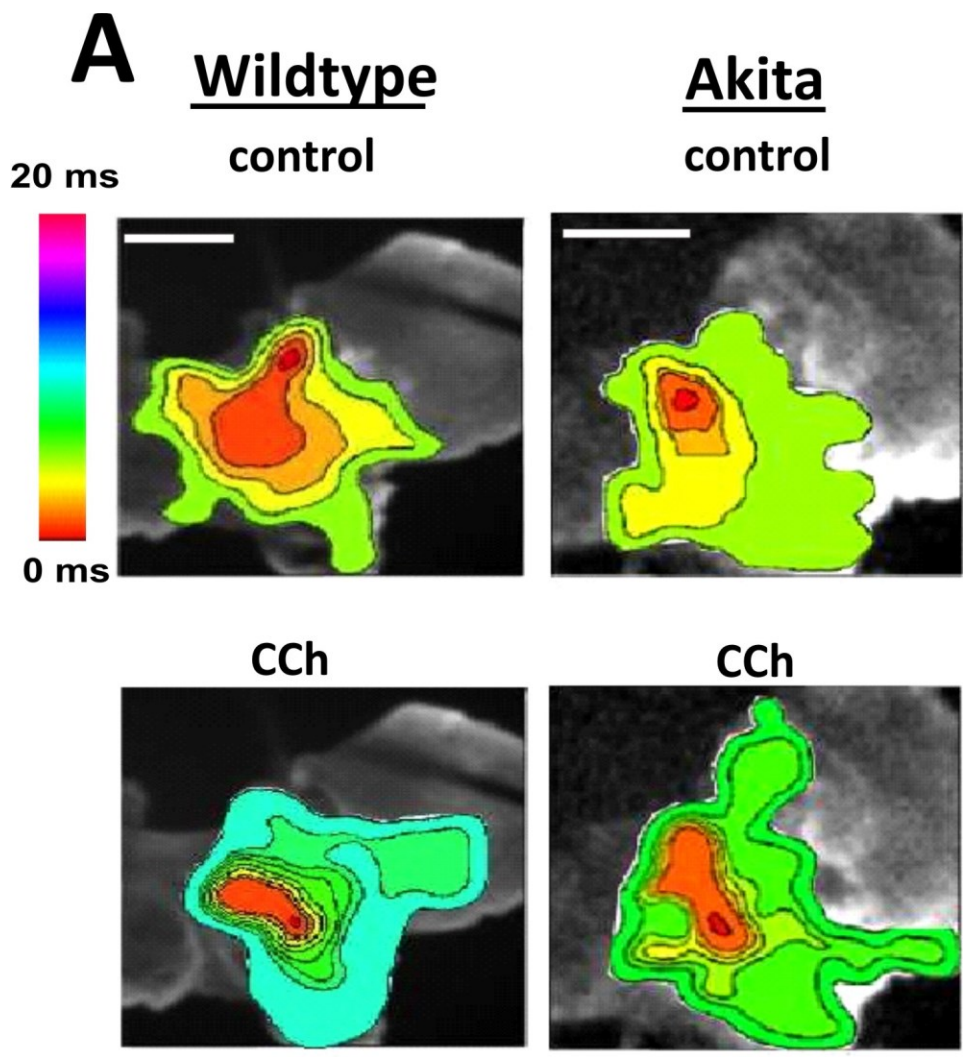

Figure 3.4

propagation in the SAN and surrounding atrial myocardium as well as the presence of preferential conduction pathways within the heterogeneous SAN region of the heart (Fedorov *et al.* 2012; Azer *et al.* 2014). Representative activation maps in control conditions demonstrate that the initial exit site was located toward the superior region of the preparation, a pattern that was seen in the majority of preparations. Application of CCh caused an inferior shift in the initial exit site as demonstrated in Figure 3.4. Importantly, and consistent with the *in vivo* data described above, the representative activation maps in Figure 3.4 show that the slowing of conduction in Akita mice was much less compared to wildtype mice after application of CCh.

These data are summarized in Figure 3.5. Since initial mapping studies were performed on atrial preparations in normal sinus rhythm the effects of CCh on cycle length were quantified. These analyses demonstrate that cycle length was increased (corresponding to a decrease in HR) after application of CCh in both wildtype (137.4 ± 4.3 ms at baseline vs. 429.5 ± 31.2 ms after CCh, $P<0.05$) and Akita (148.7 ± 4.5 ms at baseline vs. 311.1 ± 16.1 ms after CCh, $P<0.05$) (Figure 3.5A) mice; however, the magnitude of the increase is less in Akita mice (292.1 ± 29.7 ms in wildtype vs. 170.6 ± 15.4 ms in Akita, $P<0.05$) (Figure 3.5B). Local CV was measured within the initial exit site in the SAN using an established method previously described (Morley *et al.* 1999; Nygren *et al.* 2004; Azer *et al.* 2014). SAN CV was reduced after application of CCh in wildtype (9.9 ± 0.3 ms at baseline vs. 3.9 ± 0.4 ms after CCh, $P<0.05$) and Akita (8.3 ± 0.4 ms at baseline vs. 5.71 ± 0.2 ms after CCh, $P<0.05$) (Figure 3.5C) mice. The magnitude of the reduction in CV in Akita mice was significantly less than in wildtype mice (5.9 ± 0.6 ms wildtype vs. 2.6 ± 0.4 ms in Akita, $P<0.05$) (Figure

Figure 3.5: Effects of carbachol on electrical conduction in the sinoatrial node in wildtype and Akita diabetic mice in sinus rhythm A. Summary data illustrating the effects of CCh on cycle length in wildtype (n=9) and Akita diabetic (n=9) mice. *P<0.05 vs. baseline; ^{+}P<0.05 vs. wildtype. Data analyzed by two way ANOVA with Tukey's posthoc test. B. Summary data illustrating the magnitude of the increase in cycle length after application of CCh in wildtype and Akita mice. *P<0.05 vs. wildtype by Student's t-test. C. Summary data illustrating the effects of CCh on conduction velocity in the leading pacemaker site within the SAN in wildtype (n=9) and Akita diabetic (n=9) mice. *P<0.05 vs. baseline; ^{+}P<0.05 vs. wildtype. Data analyzed by two way ANOVA with Tukey's posthoc test. D. Summary data illustrating the magnitude of the reduction in SAN conduction velocity after application of CCh in wildtype and Akita mice. *P<0.05 vs. wildtype by Student's t-test.

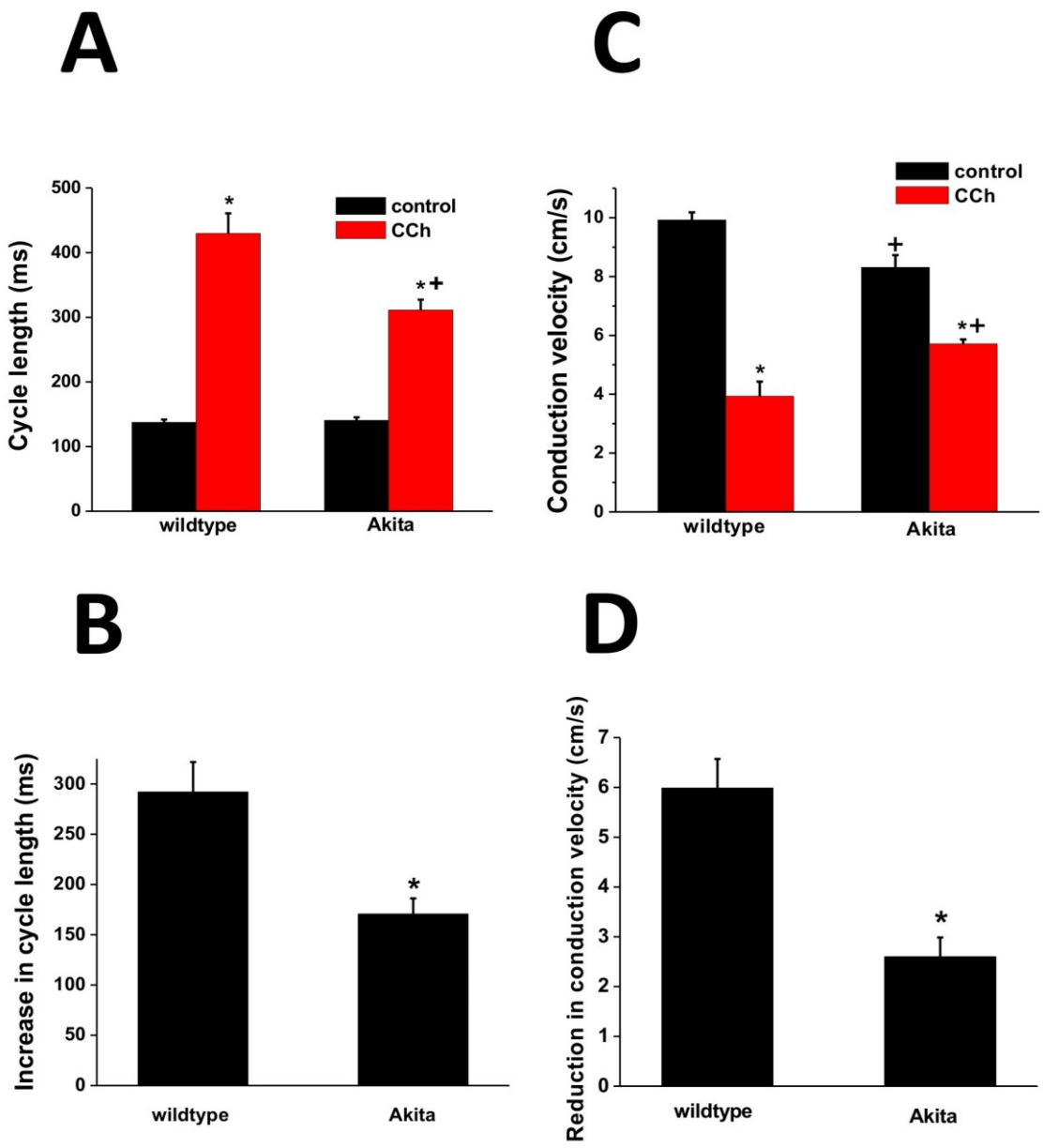
A
C
B
D
Cycle length (ms)
control
CCh
wildtype
Akita
Conduction velocity (cm/s)
Increase in cycle length (ms)
Reduction in conduction velocity (cm/s)

Figure 3.5

3.5D). Note that, as expected (Bleeker *et al.* 1980; Verheijck *et al.* 2001; Fedorov *et al.* 2006) SAN conduction velocities were consistently relatively low (i.e. less than 10 cm/s).

Optical mapping experiments were also performed in electrically paced atrial preparations to account for the possibility of rate dependent effects on CV. Atrial preparations were paced at a fixed cycle length of 120 ms. Figure 3.6 demonstrates that SAN CV is reduced in the presence of CCh in both wildtype (8.1 ± 0.6 ms at baseline vs. 3.4 ± 0.9 ms after CCh, $P<0.05$) and Akita diabetic mice (6.7 ± 0.7 ms at baseline vs. 5.1 ± 0.9 ms after CCh, $P<0.05$). Once again, the magnitude of the reduction of CV elicited by CCh in Akita mice was significantly less than in wildtype mice (4.7 ± 0.6 ms in Akita vs. 1.6 ± 0.2 ms in wildtype, $P<0.05$). These data demonstrate that the impaired parasympathetic regulation of the heart in diabetes is associated with reduced effects of CCh on electrical conduction within the SAN.

3.4 Effects of CCh on heart rate and sinus node function in insulin treated Akita diabetic mice *in vivo*

The next set of experiments was designed to investigate the role of insulin in the altered parasympathetic responsiveness of the heart in Akita diabetic mice *in vivo*. Akita mice were treated with insulin (or placebo) for 4 weeks, at which point heart rate and sinoatrial node function were assessed using intracardiac programmed stimulation. Blood glucose levels after insulin treatment were quantified and are illustrated in Figure 3.7. These measurements show insulin treatment markedly reduced blood glucose compared to placebo treated Akita mice (39.9 ± 2.1 in placebo vs. 13.3 ± 1.9 in insulin, $P<0.05$).

Figure 3.6: Effects of carbachol on electrical conduction in the sinoatrial node in paced atrial preparations from wildtype and Akita mice. Atrial preparations were paced at a fixed cycle length of 120 ms. A. Summary data illustrating the effects of CCh (0.1 μM) on SAN conduction velocity in wildtype (n=4) and Akita diabetic (n=3) mice. *P<0.05 vs. baseline; ^{+}P<0.05 vs. wildtype. Data analyzed by two way ANOVA with Tukey's posthoc test. B Summary data illustrating the magnitude of the reduction in conduction velocity after application of CCh in wildtype and Akita mice. *P<0.05 vs. wildtype by Student's t-test.

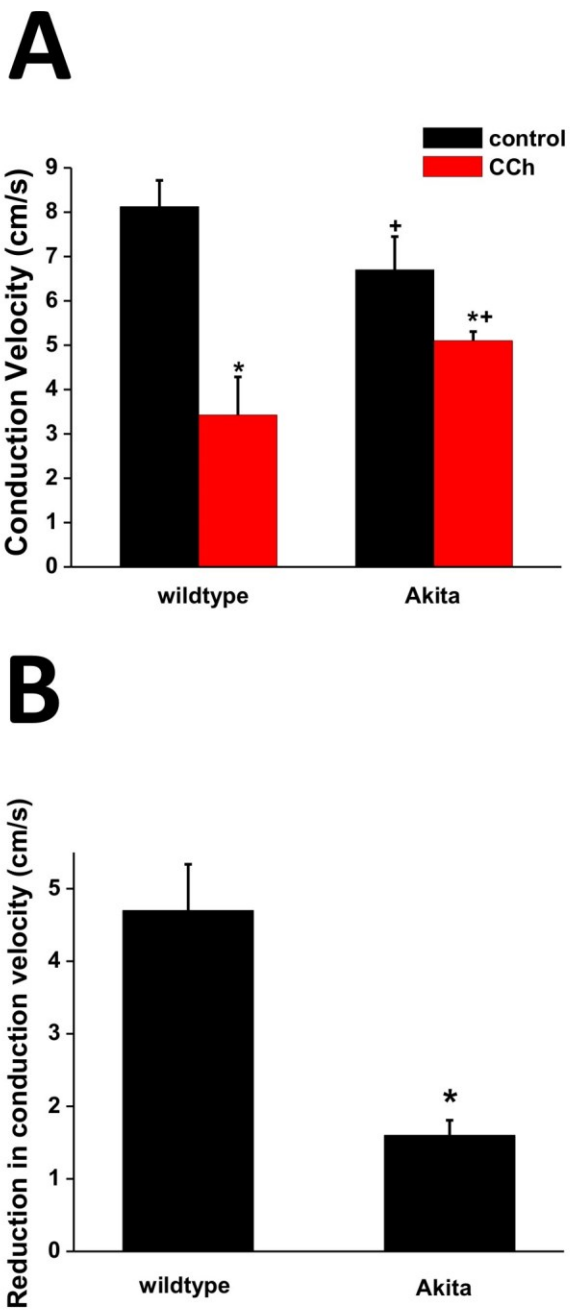
A
control
CCh
Conduction Velocity (cm/s)
0
1
2
3
4
5
6
7
8
9
*
+
*+
wildtype
Akita
B
Reduction in conduction velocity (cm/s)
0
1
2
3
4
5
*
wildtype
Akita

Figure 3.6

Figure 3.7: Blood glucose measurements in placebo and insulin treated Akita diabetic animals. Akita mice were treated with either insulin or placebo (see Methods) for 4 weeks beginning at 12 weeks of age. A. Summary data illustrating blood glucose levels for placebo and insulin treated Akita diabetic mice at 16 weeks of age. n=5 *$P<0.05$ vs. wildtype by Student's *t*-test.

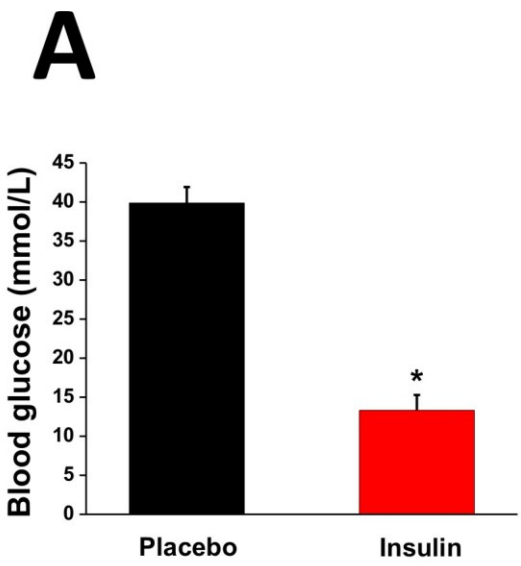
A
Blood glucose (mmol/L)
45
40
35
30
25
20
15
10
5
0
*
Placebo
Insulin

Figure 3.7

Figure 3.8: Effects of carbachol on SNRT in insulin-treated Akita diabetic mice. A. Representative ECG recordings illustrating assessment of SNRT under baseline conditions and after intraperitoneal injection (IP) of CCh (0.1 mg/kg) in anesthetized placebo-treated Akita diabetic mice. B. Representative ECG recordings illustrating the assessment of SNRT under baseline conditions and after IP injection of CCh (0.1 mg/kg) in insulin treated Akita diabetic mice. Arrows indicate first spontaneous P wave after pacing. SNRT and cSNRT values are shown for each representative recording.

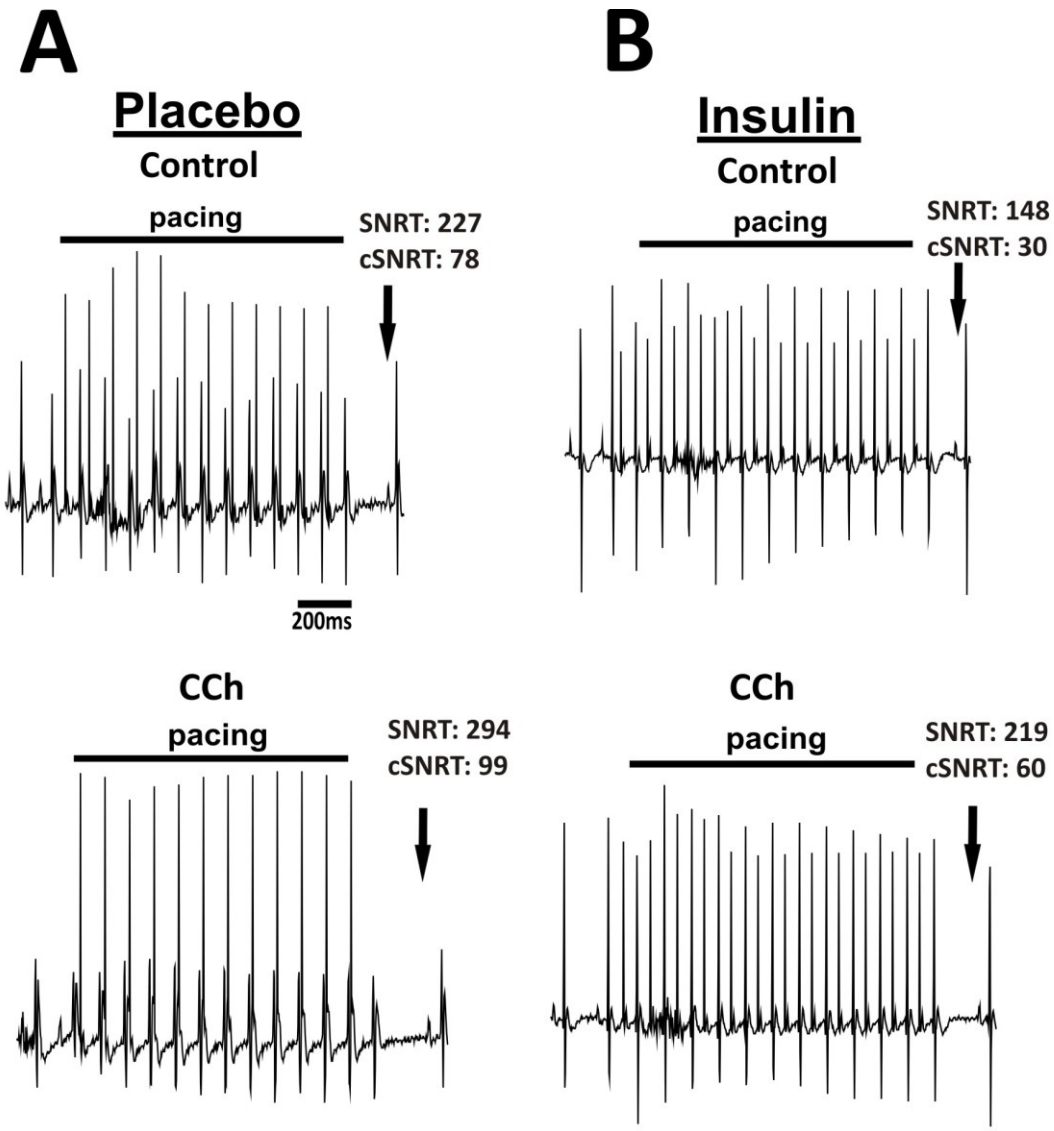
A
Placebo
Control
pacing
SNRT: 227
cSNRT: 78
200ms
CCh
pacing
SNRT: 294
cSNRT: 99
B
Insulin
Control
pacing
SNRT: 148
cSNRT: 30
CCh
pacing
SNRT: 219
cSNRT: 60

Figure 3.8

Representative ECG recordings illustrating the effects of CCh (0.1mg/kg; IP injection) on cSNRT are presented in Figure 3.8. These recordings, along with summary data (Fig 3.9) demonstrate that heart rate was reduced after CCh in both placebo (443.8 ± 17.3 beats/min at baseline vs. 366 ± 21.3 beats/min after CCh, $P<0.05$) and insulin treated (526.2 ± 7.5 beats/min at baseline vs. 356.8 ± 10.1 beats/min after CCh, $P<0.05$) (Figure 3.9A) Akita mice. Notably insulin treatment increased the magnitude of the CCh effect on heart rate compared to placebo treated mice (77.8 ± 19.9 beats/min in placebo vs. 169.3 ± 15.6 beats/min in insulin, $P<0.05$) (Figure 3.9B). In conjunction with these changes in HR, cSNRT was prolonged after application of CCh in both placebo (69.7 ± 8.9 ms at baseline vs. 84 ± 7.6 ms after CCh, $P<0.05$) and insulin treated (35.8 ± 2.4 ms at baseline vs. 67 ± 4.3 ms CCh, $P<0.05$) (Figure 3.9C) Akita mice; however, the magnitude of the increase in cSNRT was greater in insulin treated Akita diabetic mice (14.3 ± 2.7 ms in placebo vs. 31.2 ± 2.9 ms in insulin, $P<0.05$) (Figure 3.9C). Taken together these data demonstrate that insulin treatment improved the parasympathetic responsiveness seen in Akita diabetic mice.

3.5 Effects of CCh on heart rate and sinus node function in db/db type 2 diabetic mice *in vivo*

To investigate whether altered parasympathetic responsiveness of the SAN is also present in type 2 diabetes, the effects of CCh on heart rate and cSNRT were measured in db/db mice, an obese non-insulin dependent model of type 2 diabetes (Belke and Severson, 2012). Body mass and blood glucose levels were measured in db/db mice and C57BL/6 wildtype control mice (Figure 3.10). Body mass was profoundly greater in

Figure 3.9: Effects of carbachol on heart rate and sinoatrial node function in insulin-treated Akita diabetic mice *in vivo.* A. Summary data illustrating the effects of CCh (0.1 mg/kg IP) on HR in anesthetized placebo-treated (n=5) and insulin-treated (n=6) Akita diabetic mice. *P<0.05 vs. baseline; ^{+}P<0.05 vs. wildtype. Data analyzed by two way ANOVA with Tukey's posthoc test. B. Summary data illustrating the magnitude of the reduction in HR elicited by CCh in placebo-treated and insulin-treated Akita mice. *P<0.05 vs. wildtype by Student's t-test. C. Summary data illustrating the effects of CCh (0.1 mg/kg IP) on cSNRT in anesthetized placebo-treated (n=5) and insulin-treated (n=6) Akita diabetic mice. *P<0.05 vs. baseline; ^{+}P<0.05 vs. wildtype. Data analyzed by two way ANOVA with Tukey's posthoc test. D. Summary data illustrating the magnitude of the increase in cSNRT elicited by CCh in placebo-treated and insulin-treated Akita mice. *P<0.05 vs. wildtype by Student's t-test.

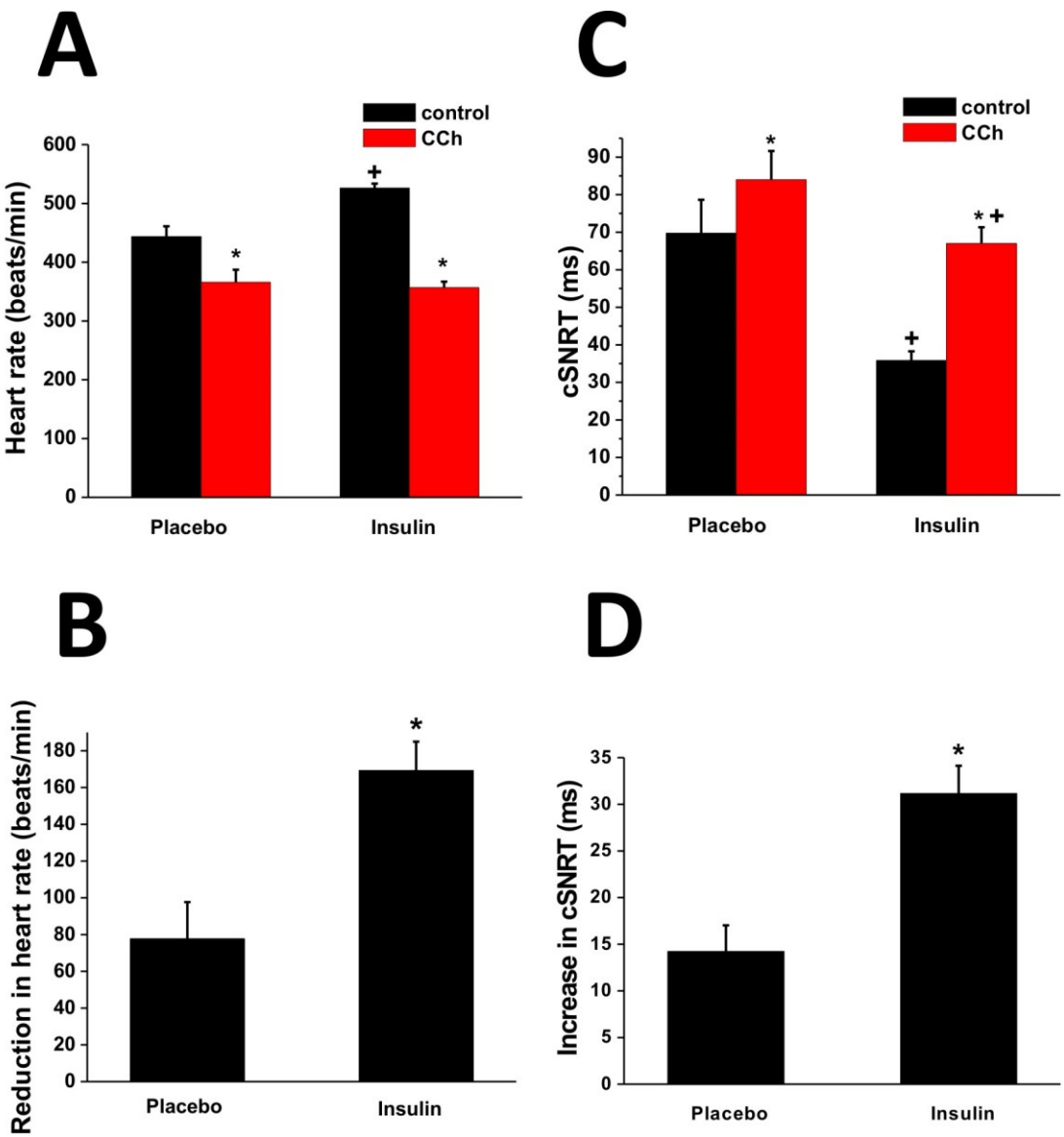
A
control
CCh
Heart rate (beats/min)
600
500
400
300
200
100
0
*
*
+
Placebo
Insulin
C
control
CCh
cSNRT (ms)
90
80
70
60
50
40
30
20
10
0
*
*+
+
Placebo
Insulin
B
Reduction in heart rate (beats/min)
180
160
140
120
100
80
60
40
20
0
*
Placebo
Insulin
D
Increase in cSNRT (ms)
35
30
25
20
15
10
5
0
*
Placebo
Insulin

Figure 3.9

Figure 3.10: Body mass and blood glucose measurements in wildtype and db/db type 2 diabetic mice. A. Summary data illustrating the body mass of wildtype and db/db diabetic mice at 16 weeks of age. n=5 *P<0.05 vs. wildtype by Student's *t*-test. B. Summary data illustrating blood glucose levels for wildtype and db/db diabetic mice at 16 weeks of age. n=5 *P<0.05 vs. wildtype by Student's *t*-test.

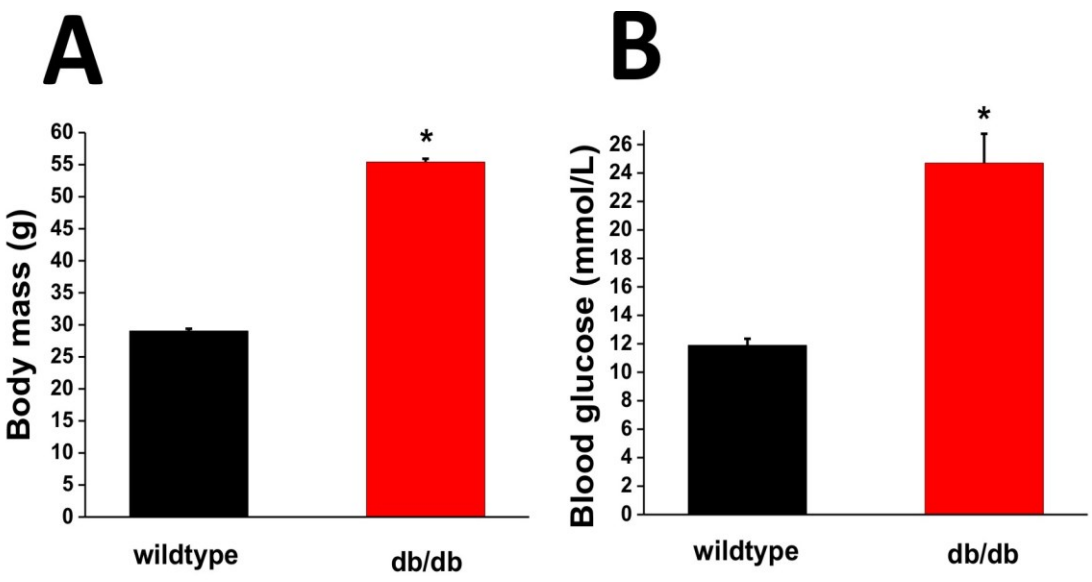
A
B
Body mass (g)
Blood glucose (mmol/L)
*
*
wildtype
db/db
wildtype
db/db

Figure 3.10

db/db mice than in wildtype mice (29.0 ± 0.3 g in wildtype vs. 55.4 ± 0.5 g in db/db, $P<0.05$) (Figure 3.10A). Similarly, blood glucose levels were elevated in db/db mice compared to wildtype controls (11.9 ± 0.4 mmol/L in wildtype vs. 24.7 ± 2.0 mmol/L in db/db, $P<0.05$) (Figure 3.10B) confirming the obese model of type 2 diabetes.

Heart rate and cSNRT were assessed before and after an IP injection of CCh (0.1mg/kg) in wildtype and db/db mice (Figure 3.11). Data summarized in Figure 3.12 demonstrates heart rate was reduced after CCh in wildtype (496.2 ± 12.0 beats/min at baseline vs. 359.4 ± 8.2 beats/min after CCh, $P<0.05$) and db/db mice (439.3 ± 6.0 beats/min at baseline vs. 342 ± 9.9 beats/min after CCh, $P<0.05$) (Figure 3.12A) as expected. Similar to Akita mice, the magnitude of the decrease in heart rate was less in db/db mice compared to wildtype mice (136.7 ± 14.5 beats/min in wildtype vs. 97.3 ± 8.9 beats/min in db/db, $P<0.05$) (Figure 3.12B). In conjunction with these effects on HR, Figures 3.11 and 3.12 demonstrate that cSNRT was prolonged in both wildtype (52.6 ± 7.6 ms at baseline vs. 92.6 ± 8.6 ms after CCh, $P<0.05$) and db/db mice (86.4 ± 7.2 ms at baseline vs. 108.1 ± 10.5 ms after CCh, $P<0.05$) (Figure 3.12C) after CCh. The magnitude of the increase in cSNRT is reduced in db/db mice compared to wildtype mice (40 ± 8.3 ms in wildtype vs. 21.8 ± 5.0 ms in db/db, $P<0.05$) (Figure3.12D). These data demonstrate that impaired parasympathetic responsiveness is present in db/db diabetic mice, similar to Akita mice.

Figure 3.11: Effects of carbachol on SNRT in db/db type 2 diabetic mice. A. Representative ECG recordings illustrating assessment of SNRT under baseline conditions and after intraperitoneal injection (IP) of CCh (0.1 mg/kg) in anesthetized wildtype mice. B. Representative ECG recordings illustrating the assessment of SNRT under baseline conditions and after IP injection of CCh (0.1 mg/kg) in db/db diabetic mice. Arrows indicate first spontaneous P wave after pacing. SNRT and cSNRT values are shown for each representative recording.

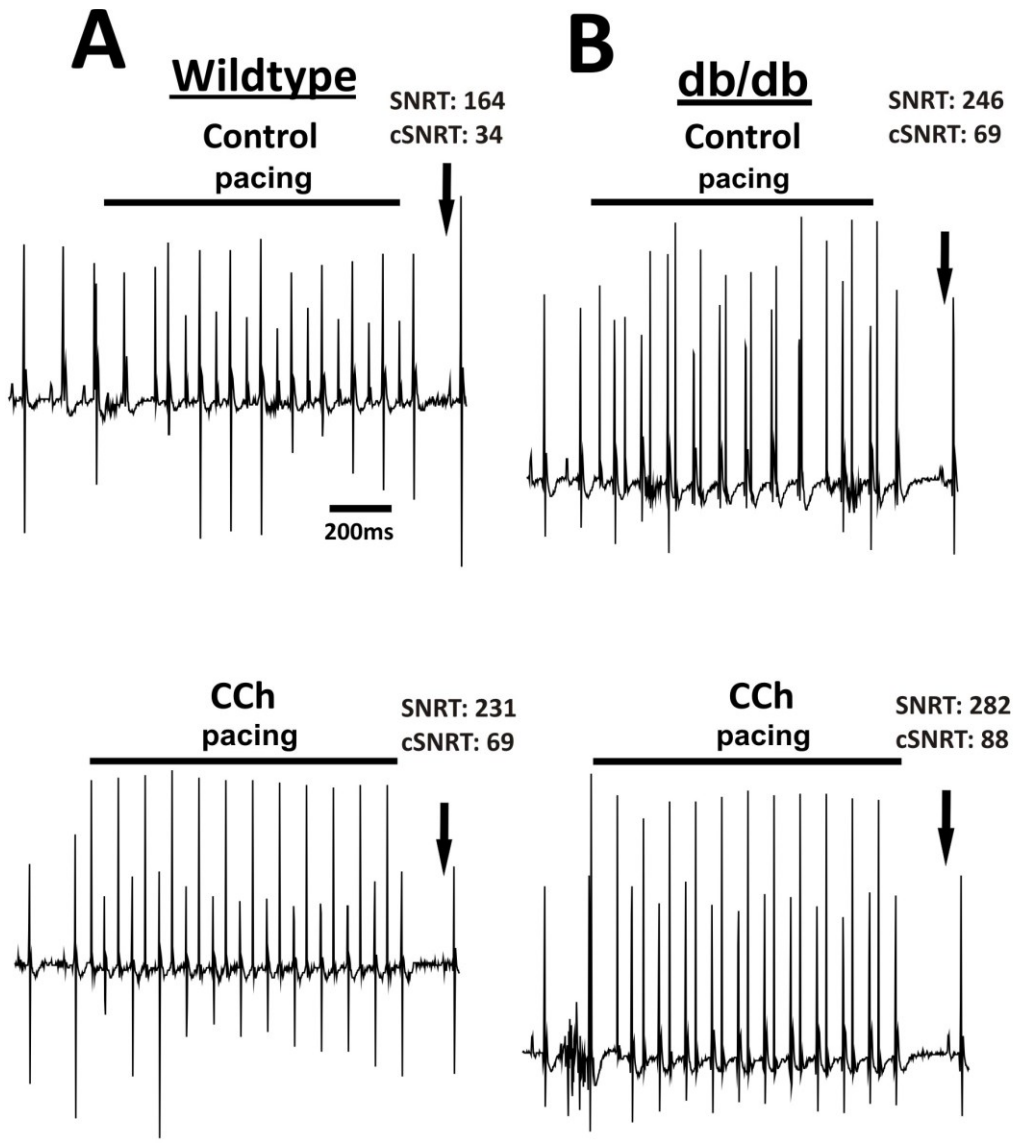
A
Wildtype
Control
pacing
SNRT: 164
cSNRT: 34
200ms
B
db/db
Control
pacing
SNRT: 246
cSNRT: 69
CCh
pacing
SNRT: 231
cSNRT: 69
CCh
pacing
SNRT: 282
cSNRT: 88

Figure 3.11

Figure 3.12: Effect of carbachol on heart rate and sinoatrial node function in db/db type 2 diabetic mice *in vivo.* A. Summary data illustrating the effects of CCh (0.1 mg/kg IP) on HR in anesthetized wildtype (n=9) and db/db (n=13) mice. *P<0.05 vs. baseline; ^{+}P<0.05 vs. wildtype. Data analyzed by two way ANOVA with Tukey's posthoc test. B. Summary data illustrating the magnitude of the reduction in HR elicited by CCh in wildtype and db/db mice. *P<0.05 vs. wildtype by Student's t-test. C. Summary data illustrating the effects of CCh (0.1 mg/kg IP) on cSNRT in anesthetized wildtype (n=9) and db/db (n=13) mice. *P<0.05 vs. baseline; ^{+}P<0.05 vs. wildtype. Data analyzed by two way ANOVA with Tukey's posthoc test. D. Summary data illustrating the magnitude of the increase in cSNRT elicited by CCh in wildtype and db/db mice. *P<0.05 vs. wildtype by Student's t-test.

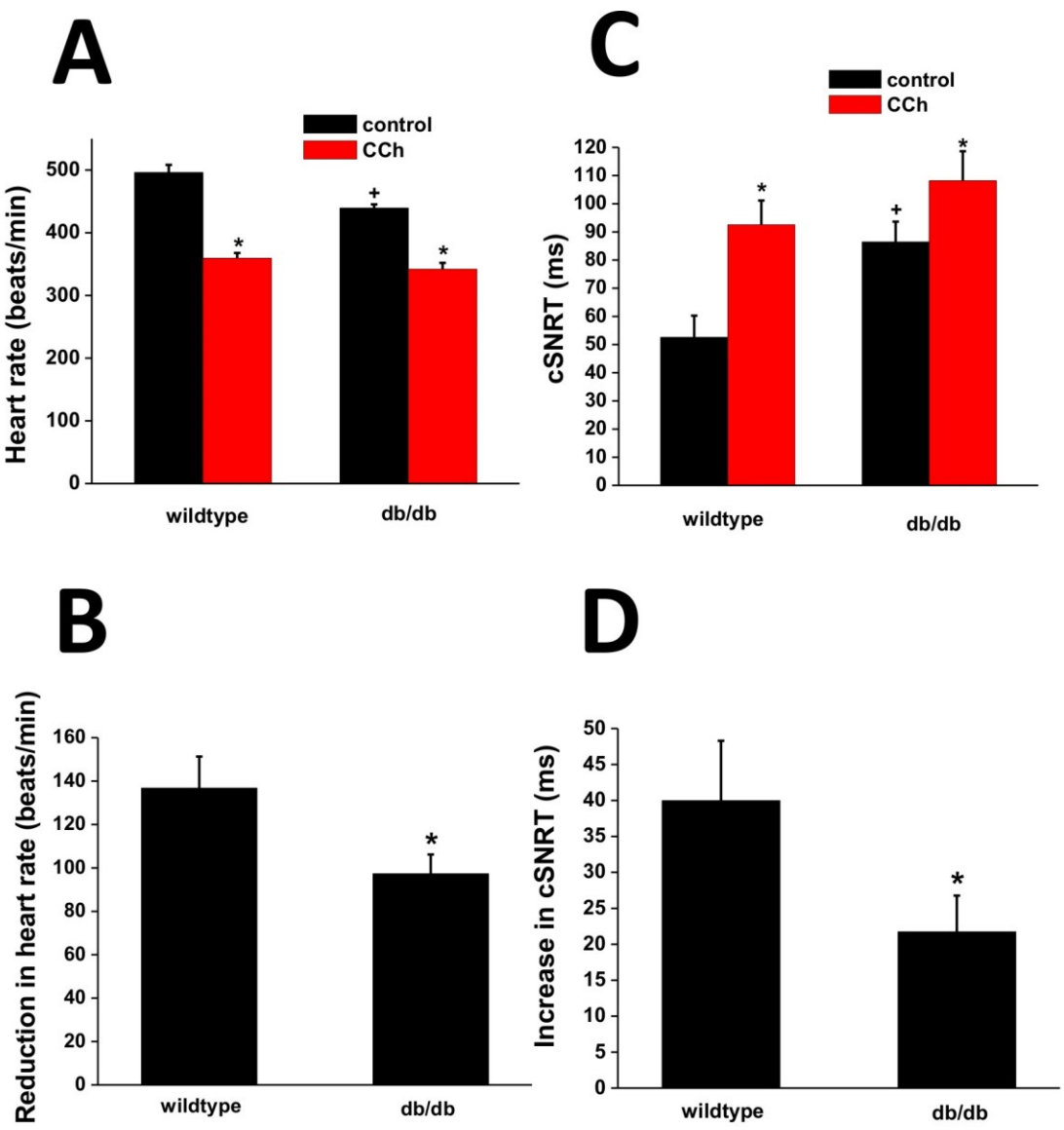
A
control
CCh
Heart rate (beats/min)
500
400
300
200
100
0
*
+
*
wildtype
db/db
C
control
CCh
cSNRT (ms)
120
110
100
90
80
70
60
50
40
30
20
10
0
*
+
*
wildtype
db/db
B
Reduction in heart rate (beats/min)
160
140
120
100
80
60
40
20
0
*
wildtype
db/db
D
Increase in cSNRT (ms)
50
45
40
35
30
25
20
15
10
5
0
*
wildtype
db/db

Figure 3.12

Figure 3.13: Effects of carbachol on patterns of electrical conduction in the sinoatrial node in db/db type 2 diabetic mice. A. Representative colour maps showing activation patterns in control conditions and after application of CCh (0.1 μM) in wildtype and db/db diabetic mice. In these figures the right atrial appendage is on the right side of the image. Red colour indicates earliest activation time (ms) in the SAN within the right atrial posterior wall. Time interval between successive isochrones is 1 ms. Scale bars are 2 mm.

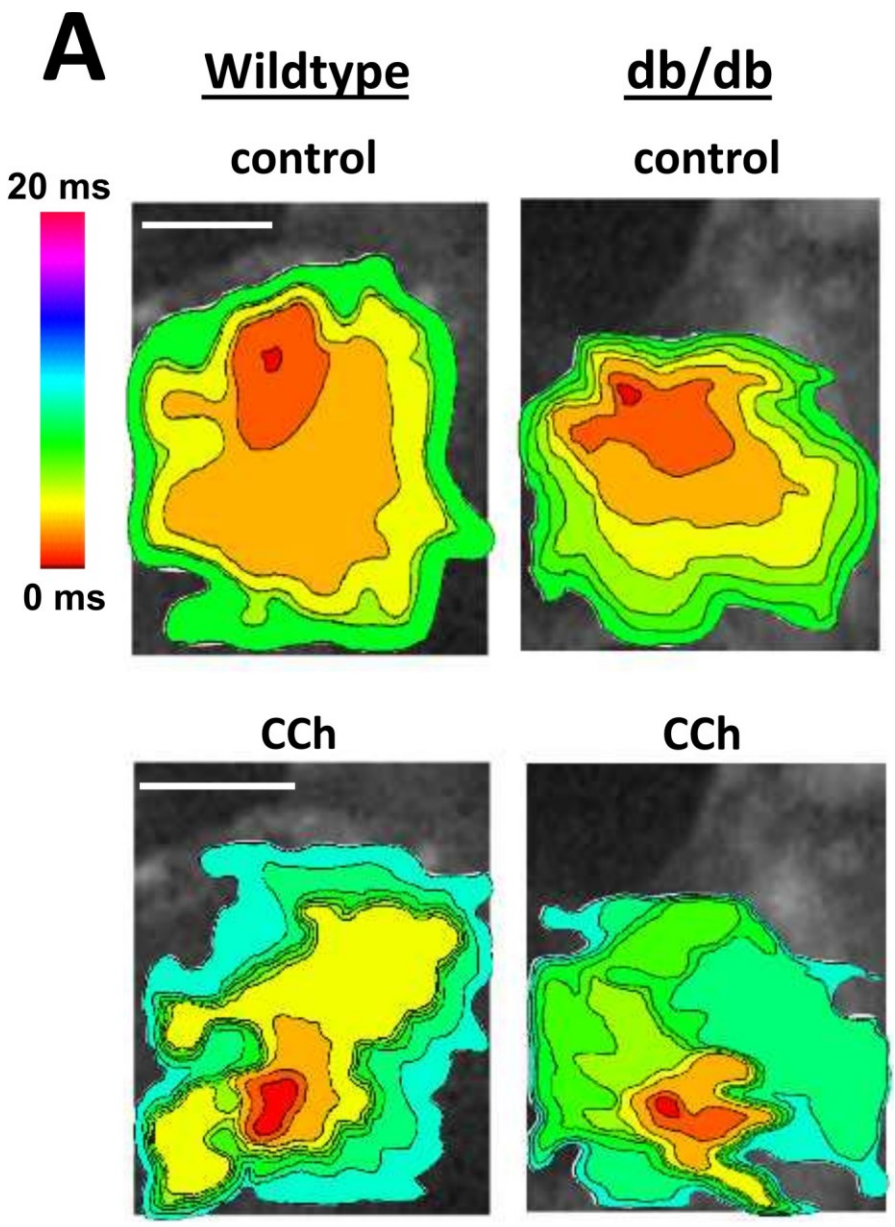

Figure 3.13

3.6 Effects of CCh on patterns of electrical conduction in the sinoatrial node in db/db type 2 diabetic mice.

High-resolution optical mapping was used to evaluate the effects of parasympathetic activation on patterns of electrical conduction in the SAN in db/db mice. As described above, these studies were performed by applying CCh (0.1 μM) in isolated atrial preparations.

Figure 3.13 demonstrates representative color maps showing activation patterns in wildtype and db/db mice. Application of CCh elicits a clear slowing of electrical conduction from the SAN through the right atrial posterior wall in both wildtype and db/db mice; however, the effect is smaller in db/db hearts. Representative maps also demonstrate in control conditions that the initial exit site was located toward the superior region of the preparation, which was seen in the majority of preparations. Application of CCh caused an inferior shift in the initial exit site.

These mapping studies in db/db mice were performed in sinus rhythm. Figure 3.14 demonstrates cycle length is prolonged after application of CCh in both wildtype (134 ± 5.4 ms at baseline vs. 435.8 ± 23.9 ms after CCh, $P<0.05$) and db/db (152.6 ± 12.0 ms at baseline vs. 327.3 ± 14.8 ms after CCh, $P<0.05$) (Figure 3.14A) mice, and that the magnitude of the increase in cycle length was smaller in db/db mice than in wildtype mice (301.9 ± 25.3 ms in wildtype vs. 174.7 ± 14.2 ms in db/db, $P<0.05$) (Figure 3.14B). CV was also decreased after application of CCh in both wildtype (8.4 ± 0.4 ms at baseline vs. 4.0 ± 0.5 ms after CCh, $P<0.05$) and db/db (7.6 ± 0.4 ms at baseline vs. 4.8 ± 0.2 ms after CCh, $P<0.05$) (Figure 3.14C) mice. Once again, the magnitude of the decrease in CV was less in db/db mice than in wildtype mice (4.3 ±

Figure 3.14: Effects of carbachol on electrical conduction in the sinoatrial node in wildtype and db/db type 2 diabetic mice. A. Summary data illustrating the effects of CCh on cycle length in wildtype (n=9) and db/db diabetic (n=13) mice. *P<0.05 vs. baseline; ^{+}P<0.05 vs. wildtype. Data analyzed by two way ANOVA with Tukey's posthoc test. B. Summary data illustrating the magnitude of the increase in cycle length after application of CCh in wildtype and db/db mice. *P<0.05 vs. wildtype by Student's t-test. C. Summary data illustrating the effects of CCh on conduction velocity in the leading pacemaker site in wildtype (n=9) and db/db diabetic (n=13) mice. *P<0.05 vs. baseline; ^{+}P<0.05 vs. wildtype. Data analyzed by two way ANOVA with Tukey's posthoc test. D. Summary data illustrating the magnitude of the reduction in conduction velocity after application of CCh in wildtype and db/db mice. *P<0.05 vs. wildtype by Student's t-test.

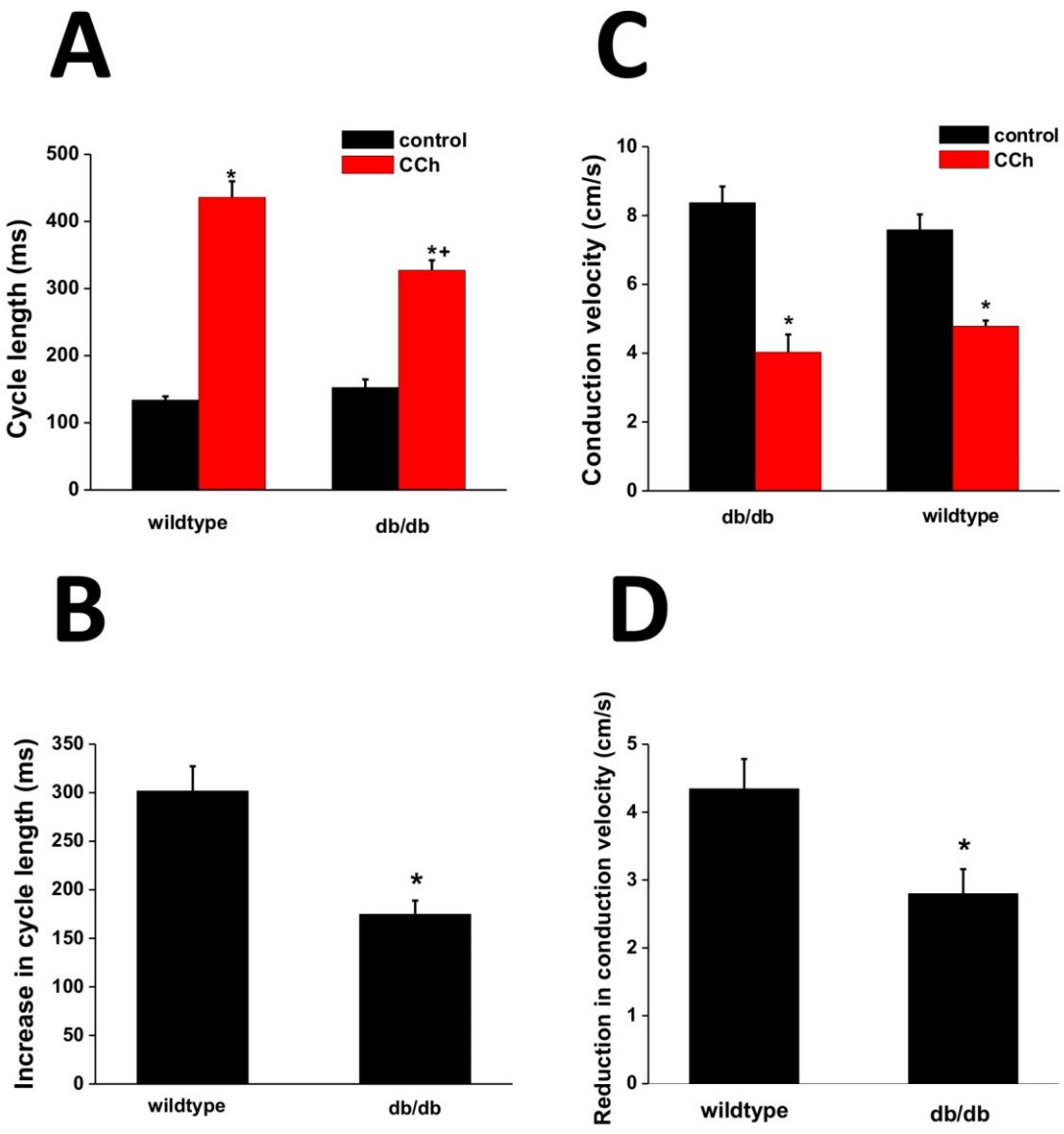
A
control
CCh
Cycle length (ms)
500
400
300
200
100
0
*
*+
wildtype
db/db
C
control
CCh
Conduction velocity (cm/s)
10
8
6
4
2
0
*
*
db/db
wildtype
B
Increase in cycle length (ms)
350
300
250
200
150
100
50
0
*
wildtype
db/db
D
Reduction in conduction velocity (cm/s)
5
4
3
2
1
0
*
wildtype
db/db

Figure 3.14

0.4 ms in wildtype vs. 2.8 ± 0.4 ms in db/db, $P<0.05$) (Figure 3.14D). These finding illustrate that, similar to type 1 diabetic Akita mice, the effects of CCh on electrical conduction in the SAN are impaired in type 2 diabetic db/db hearts.

3.7 Effects of Iso on electrical conduction in the sinoatrial node in isolated atrial preparations.

Finally, a preliminary set of studies was conducted, using high-resolution optical mapping, to determine whether sympathetic responsiveness of the SAN was also altered in diabetes. Sympathetic regulation of HR is known to be impaired in diabetic patients (Ziegler, 1994; Vinik and Ziegler, 2007). These studies were performed using wildtype and Akita hearts in which the β-adrenergic receptor agonist isoproterenol (ISO; 10 nM) was applied as a sympathetic agonist.

Figure 3.15 demonstrates representative color maps showing activation patterns in wildtype and Akita mice before and after application of ISO. Conduction is increased after application of ISO in both wildtype and Akita animals (note the smaller number of contour lines spaced further apart following application of ISO); however the effect is less pronounced in Akita hearts. These representative maps demonstrate in control conditions that the initial exit site was located in the inferior SAN region of the preparation. Application of ISO caused a superior shift in the initial exit site in wildtype mice however this shift was not apparent in the Akita mice.

Summary data (Figure 3.16) demonstrate that cycle length was shortened after application of ISO in both wildtype (154.1 ± 4.7 ms at baseline vs. 79.9 ± 2.0 ms after ISO, $P<0.05$) and Akita (147.6 ± 3.6 ms at baseline vs. 85.8 ± 4.2 ms after ISO, $P<0.05$)

(Figure 3.16A) mice. The magnitude of the reduction in cycle length after ISO is smaller in Akita mice than in wildtype mice (74.2 ± 3.8 ms in wildtype vs. 61.8 ± 2.6 ms in Akita, $P<0.05$) (Figure 3.16B). Conduction velocity within the leading exit site in the SAN was increased after application of ISO in both wildtype (5.9 ± 0.2 ms at baseline vs. 10.4 ± 0.6 ms after ISO, $P<0.05$) and Akita (6.0 ± 0.3 ms at baseline vs. 8.6 ± 0.3 ms after ISO, $P<0.05$) (Figure 3.16C) mice; however, the magnitude of the increase in conduction velocity was smaller in Akita mice compared to wildtype mice (4.5 ± 0.5 ms in wildtype vs. 2.6 ± 0.6 ms in Akita, $P<0.05$) (Figure 3.16D). These data show that Akita mice also demonstrate altered responses to ISO.

Figure 3.15: Effects of isoproternol on patterns of electrical conduction in the sinoatrial node in Akita diabetic mice. A. Representative colour maps showing activation patterns in control conditions and after application of ISO (10 nM) in wildtype and Akita diabetic mice. In these figures the right atrial appendage is on the right side of the image. Red colour indicates earliest activation time (ms) in the SAN within the right atrial posterior wall. Time interval between successive isochrones is 1 ms. Scale bars are 2 mm.

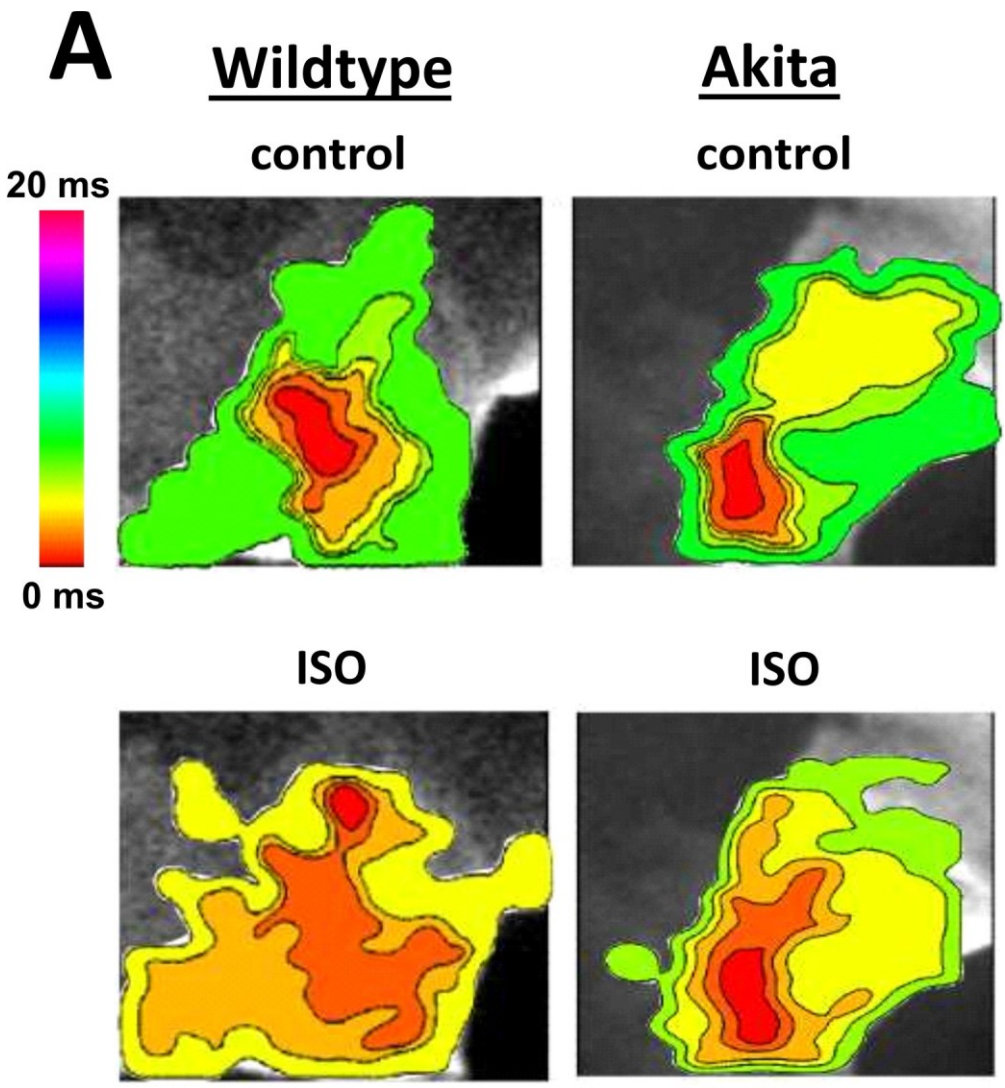

Figure 3.15

Figure 3.16: Effects of isoproterenol on electrical conduction in the sinoatrial node in Akita diabetic mice A. Summary data illustrating the effects of ISO on cycle length in wildtype (n=9) and Akita diabetic (n=9) mice. *P<0.05 vs. baseline; ^{+}P<0.05 vs. wildtype. Data analyzed by two way ANOVA with Tukey's posthoc test. B. Summary data illustrating the magnitude of the increase in cycle length after application of ISO in wildtype and Akita mice. *P<0.05 vs. wildtype by Student's t-test. C. Summary data illustrating the effects of ISO on conduction velocity in the leading pacemaker site in wildtype (n=9) and Akita diabetic (n=9) mice. *P<0.05 vs. baseline; ^{+}P<0.05 vs. wildtype. Data analyzed by two way ANOVA with Tukey's posthoc test. D. Summary data illustrating the magnitude of the reduction in conduction velocity after application of ISO in wildtype and Akita mice. *P<0.05 vs. wildtype by Student's t-test

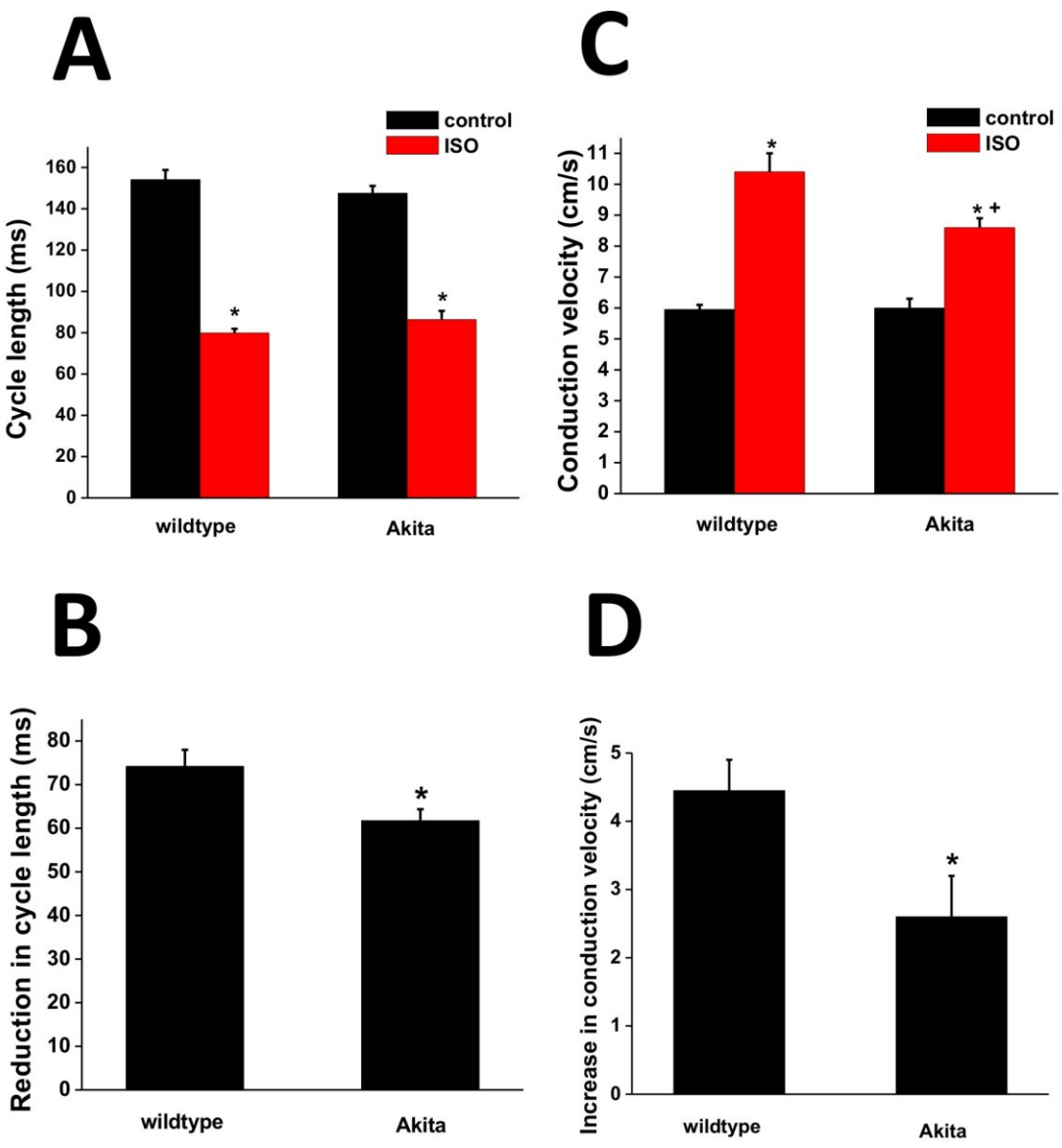
A
control
ISO
Cycle length (ms)
160
140
120
100
80
60
40
20
0
*
*
wildtype
Akita
C
control
ISO
Conduction velocity (cm/s)
11
10
9
8
7
6
5
4
3
2
1
0
*
* +
wildtype
Akita
B
Reduction in cycle length (ms)
80
70
60
50
40
30
20
10
0
*
wildtype
Akita
D
Increase in conduction velocity (cm/s)
5
4
3
2
1
0
*
wildtype
Akita

Figure 3.16

CHAPTER 4: DISCUSSION

4.1 Overview of Key Findings

Is has previously been demonstrated in both basic and clinical research that autonomic regulation of heart rate in diabetes is impaired (Vinik and Ziegler, 2007; Park *et al.* 2009). Heart rate is determined by the intrinsic spontaneous activity of the SAN and is critically regulated by the autonomic nervous system (PSNS and SNS), which abundantly innervates the SAN. We hypothesized that altered parasympathetic responsiveness of the heart in diabetes is related to alterations within the SAN how it responds to parasympathetic agonists. Our data demonstrate that the parasympathetic activation of the SAN via CCh is blunted in both Akita mice and db/db mice *in vivo*. Specifically, the ability of CCh to slow HR and elongate cSNRT was reduced in both mouse models of diabetes. To determine the mechanism for these *in vivo* responses, we used high-resolution optical mapping to study electrical conduction and found that diabetic mice show impaired parasympathetic responses within the SAN. In these studies, CCh was applied to isolated atrial preparations in which we can map patterns of electrical conduction specifically in the SAN. Consistent with our *in vivo* data, the ability of CCh to slow CV and increase cycle length in the SAN was reduced in diabetic hearts. A separate set of *in vivo* work demonstrated that a 4 week insulin treatment period was able to reverse the impaired parasympathetic responsiveness in Akita diabetic mice, as indicated by the reversal of HR and cSNRT responses to CCh to levels similar to measurements obtained in wildtype littermates. Lastly, we used high-resolution optical mapping to investigate possible impaired responses of the SAN to the sympathetic agonist ISO. These data demonstrate that ISO had a reduced ability to increase CV and

shorten cycle length in the SAN of isolated Akita diabetic hearts. These data present interesting and novel contributions to the study of altered autonomic regulation of heart rate in diabetes

4.2 Impaired parasympathetic responsiveness of the sinoatrial node in diabetic mice

In clinical settings diabetic cardiovascular autonomic neuropathies tend to present in diabetic patients after several years of living with the disease. Thus it is often thought of as a progressive complication pertaining to a later stage of the disease (Vinik and Ziegler, 2007). Despite its prevalence and severity, the underlying mechanisms that lead to the development of impaired autonomic regulation of heart rate are poorly understood. Our work proposes a key component involved in the early stage development of cardiovascular autonomic neuropathy in diabetes.

Parasympathetic control of heart rate consists of a neural component, carrying input from the central nervous system, and an intrinsic cardiac molecular response pathway. In the present study we used the Akita mouse model of type 1 diabetes to investigate whether altered parasympathetic regulation of HR seen in diabetic patients could be attributed to alterations in how the SAN responds to parasympathetic agonists. Our measurements of HR in response to CCh *in vivo* demonstrate that CCh had a reduced ability to slow heart rate in Akita diabetic mice in association with a reduced ability to elongate cSNRT. Taken together these data show that the Akita mouse model displays the impaired parasympathetic regulation of HR seen in diabetics and further demonstrate that this is due, at least in part, to changes in the responsiveness of the SAN to CCh.

Our data are consistent with what has previously been reported by Park *et al.* (2009) and Zhang *et al.* (2014). They demonstrated that the negative chronotropic

response to CCh was blunted in Akita diabetic mice compared to wildtype (but did not investigate the role of the SAN in this response).

Impaired parasympathetic control of the heart in diabetes has been described in a number of studies. McDowell *et al.* (1994) demonstrated that diabetic rabbits have a significant impairment in the parasympathetic mediated baroreceptor control of heart rate. Similarly, diabetic rats also demonstrate a significant impairment of parasympathetic control of heart rate reflected by lower HRV (Fazan *et al.* 1997). These effects are consistent with findings in humans, where it has been shown T1D patients reflect significant impairments in parasympathetic control of heart rate (Javorka *et al.* 2005).

However many of these studies have attributed cardiovascular autonomic dysfunction in diabetes with damage or degeneration of autonomic nerve fibers that innervate the heart, including the SAN. More recently, specific intrinsic alterations within the diabetic heart and its responsiveness to autonomic signaling have been implicated (Van Buren *et al.* 1998; Park *et al.* 2009; Zhang *et al.* 2014). In one study, ECG data from STZ-induced diabetic rats demonstrated that diabetic rats demonstrated a reduced HR response to vagal stimulation. Furthermore they show that neurogenic factors are of little importance in the impaired parasympathetic control as treatment with a neurotrophic factor (Org 2766) did not reverse the impairment (Van Buren *et al.* 1998). Another study by Mabe and Hoover (2010) found that HR responses to vagal nerve stimulation in STZ-induced diabetic mice were blunted *in vivo*, but that these blunted responses were not seen in the presence of cholinergic agonists in isolated right atria. Although they hypothesized that impaired parasympathetic responses were due to nerve

fiber damage, they found no difference in abundance of cholinergic nerve fibers in diabetic hearts.

Changes in SNRT have been investigated in a number of experimental settings using both animal and human models (Narula *et al.* 1972; Chadda *et al.* 1975; Tonkin *et al.* 1980). Both prolongation and shortening of SNRT can be pathological and representative of sinus node dysfunction depending on the conditions these alterations occur in (Narula *et al.* 1972; Chadda *et al.* 1975; Tonkin *et al.* 1980; Nalos et al. 1986). Much of the research on SNRT has demonstrated the negative associations of prolongation of SNRT. A prolonged SNRT is commonly associated with an increased risk of atrial fibrillation (Elvan et al. 1996). Prolongation of SNRT indicates an inability of the SAN to correctly resume regular impulse propagation. The effects of a shortened SNRT are not as widely documented, but have been associated with pathological phenomenon like sinus node exit block (Nalos et al. 1986). Our data demonstrate that the prolongation of SNRT in response to cholinergic stimulation is blunted in diabetic mice. This response may reflect an impaired ability of the SAN to properly correct for physiological changes in HR in diabetes. Impaired SAN activity in diabetes could be linked to the increase in harmful arrhythmias seen in diabetes (Davies et al 1998).

We next conducted a series of experiments to further explore altered responsiveness of the SAN to CCh in diabetes by investigating electrical activation patterns and electrical conduction in the SAN. We used high-resolution optical mapping to study the effects of CCh on patterns of electrical conduction in the SAN as well as on SAN cycle length and CV. CCh showed a reduced capacity to slow electrical conduction in the SAN and right atrial posterior wall in Akita hearts. Consistent with our

measurements of HR and SAN function *in vivo*, the effects of CCh on cycle length (i.e. HR) were blunted in atrial preparations used for optical mapping studies from Akita mice. Since CV is partially dependent on HR, we measured SAN conduction in atrial preparations in sinus rhythm as well as during pacing at a fixed cycle length. In both instances CCh had a reduced ability to slow SAN CV in Akita hearts, suggesting that this is a critical contributor to the impaired responsiveness of the SAN to parasympathetic agonists in the diabetic heart.

A major mechanism by which CCh inhibits SAN activity is by slowing electrical conduction within the SAN (Federov *et al.* 2006; Glukhov *et al.* 2010). Parasympathetic activation results in a number of ion channel effects in the SAN including inhibition of $I_{Ca,L}$ and I_f as well as activation of I_{kACh} (Irisawa *et al.* 1993; Kodama *et al.* 1996; Federov *et al.* 2006). Several of these effects, including a reduction in $I_{Ca,L}$ in particular, could lead to a reduction in the AP upstroke velocity, which is a key determinant of conduction velocity (Lakatta *et al.* 2010). One study demonstrated that $I_{Ca,L}$ (in ventricular myocytes) is reduced in Akita diabetic mice as a result of reduced phosphatidylinositol-4,5-bisphosphate 3-kinase (PI3K) signaling (Lu *et al.* 2007). This result was proposed to be a consequence of defective insulin signaling, as PI3Ks are critical mediators of insulin action (Oudit *et al.* 2004). It is presently unknown if $I_{Ca,L}$ is altered in the SAN; however, if it is, this would be consistent with our observation that the CV response to CCh in diabetic animals is impaired since changes in the upstroke are considered to be major contributors to changes in CV of the SAN. This also supports our finding that CCh increases cycle length and that the response is blunted in diabetic mice as the activation of I_{KACh} and subsequent hyperpolarization of the cell is associated with

increases in cycle length (Federov *et al.* 2006). Thus altered parasympathetic responsiveness of the SAN in diabetes would likely encompass altered I_{kACh} regulation of electrical conduction.

T2D is the most common type of diabetes, and its prevalence continues to rise worldwide. A significant number of T2D patients are affected by CAN however much less is known about the etiology of impaired autonomic regulation of the heart in the setting of T2D.To investigate if the altered parasympathetic responsiveness of the SAN in T1D was also present in T2D we used the db/db mouse model. Similar to our previous *in vivo* data in Akita mice, measurements of the effects of CCh on HR and cSNRT *in vivo* demonstrate that db/db mice also possess impaired parasympathetic regulation of HR and that these alterations are potentially related to intrinsic alterations in SAN responsiveness to CCh.

Similarly, da Costa Goncalves *et al.* (2009) demonstrated that db/db mice possess features seen in type 2 diabetic autonomic neuropathy, specifically that blood pressure responses, HRV, and parasympathetic tone are impaired in the db/db mouse. Human studies of T2D indicate that insulin resistance may also be associated with impaired parasympathetic regulation of the heart, specifically altered HRV (Perciaccante *et al.* 2006), and blunted parasympathetic effects on heart rate (Banthia *et al.* 2012).

The mechanisms of insulin resistance are complex and still not completely understood, consequently neither is the etiology of cardiovascular autonomic neuropathy in the setting of T2D. Our data provide new insight into the mechanisms responsible for impaired parasympathetic regulation of heart rate seen in T2D patients, specifically implicating intrinsic alterations in the responses of the SAN.

In accordance with our previous experiments, we used high-resolution optical mapping to investigate the effects of CCh on activation patterns, SAN CV and cycle length in db/db mice. CCh consistently showed a reduced capacity to slow electrical conduction in the SAN and in db/db hearts. In conjunction with this and consistent with our results from Akita diabetic animals, the effects of CCh on cycle length were blunted in the atrial preparations from db/db mice. These data are consistent with our *in vivo* data of HR and cSNRT in db/db mice and further demonstrate the presence of impaired SAN responsiveness to CCh in T2D.

Our data demonstrate similar findings in both T1D and T2D mice. The magnitude of the HR and cSNRT response elicited by CCh were reduced compared to wildtype controls in both Akita and db/db mice. These effects were mimicked by our optical mapping data which demonstrated that the magnitude of the CV and cycle length response to CCh application was also reduced compared to wildtype in both Akita and db/db mice. These impaired parasympathetic effects are also seen in human patients with T1D and T2D (Ewing and Clarke, 1982; Javorka et al. 2005). The most prominent presentation of this alteration in humans is impaired HRV responses (Javorka et al. 2005). Our results indicate that the difference in the magnitude of response in Akita mice is greater than the differences in the magnitude of responses in db/db mice. We have speculated that the impaired parasympathetic effects could be in part related to alterations of downstream effectors of insulin signaling. Therefore it is possible that this difference in the responses of T1D and T2D mice could be due to the fact that in T1D there is a complete lack of insulin, and that in T2D some insulin is still present. These results however are contradictory to what is typically seen in human patients, whereby it has

been reported that impairments in parasympathetic regulation of the heart in humans are thought to be more severe in T2D (Vinik and Ziegler, 2007; Karayannis et al. 2012). Autonomic tone and HR control is different in mice than in humans. In mice it has been demonstrated that sympathetic tone dominates the control of HR (Swoap et al. 2008) whereas it has been shown that parasympathetic tone dominates the control of HR in humans (Robinson et al. 1966). This difference in HR control could contribute to some of the differences seen in the severity of autonomic neuropathy in mice versus humans.

4.3 Insulin treatment improves impaired responsiveness to carbachol in Akita diabetic mice *in vivo*

It is widely recognized that insulin administration is the number one treatment for T1D. To investigate the effects of insulin treatment on impaired CCh effects in the Akita mouse we treated a group of animals with insulin pellets for 4 weeks. Our data demonstrate the impaired effects of CCh on HR and cSNRT were completely reversible following insulin treatment. This is consistent with the previous work of Park *et al.* (2009) who demonstrated that insulin treatment rescues the impaired HR response to CCh *in vivo*

In a study of T1D patients, individuals who were placed on an intensive insulin treatment demonstrate a slower progression of CAN. In some patients insulin even prevented the development of CAN (Pop-Busui *et al.* 2009). In this DCCT trial, the intensive treatment group of patients demonstrated a reduced incidence of CAN by 50% over 6.5 years follow-up compared with conventional therapy (twice a day standard injections of insulin; not delivered through a pump) (Pop-Busui *et al.* 1998; 2009).

Our data present novel findings suggest that impaired parasympathetic regulation of HR in diabetes could in part be attributes to alterations in the downstream effectors of insulin signaling pathways and their role in the parasympathetic modulation of the SAN.

4.4 Impaired sympathetic responsiveness of the sinoatrial node to isoproterenol in Akita diabetic mice

The present study has largely focused on impaired parasympathetic responsiveness of the SAN in diabetes. However, it has also been demonstrated that sympathetic regulation of the heart in diabetes is also altered (Ziegler, 1994; Vinik and Ziegler, 2007). We began to investigate possible alterations in sympathetic responsiveness of the SAN using high-resolution optical mapping to look at SAN conduction in response to ISO. Our measurements indicate that, similar to the blunted effects of CCh, ISO demonstrated a reduced ability to increase CV in the SAN. ISO also showed blunted effects in its ability to reduce cycle length (i.e. increase HR).

In normal conditions, ISO acts to increase SAN activity by speeding electrical conduction (Glukhov *et al.* 2010). Consistent with our measurements, Luo *et al.* (2013) investigated SAN function in the context of oxidant stress, and showed that STZ-treated mice showed impaired HR responses to ISO. There has been evidence from both basic and clinical studies implicating the presence of abnormal SNS signaling in the diabetic heart. Impaired sympathetic responsiveness in the heart has been shown in the form of blunted baroreceptor adrenergic reflexes in adult diabetic rats (Schreihofer *et al.* 2007). Rats demonstrate a reduced sympathetic reflex control of HR compared with wildtype controls. Dincer *et al.* (2001) has demonstrated decreased responsiveness of the heart to ß adrenergic receptors agonists in STZ-induced rats. They also show evidence of down

regulation of ß adrenergic receptors in diabetic rat hearts (Dincer *et al.* 2001). As we previously addressed, many studies on sympathetic dysfunction in diabetes have focused on neuronal changes. Once again, our data show clear alterations of conduction patterns in isolated SAN atrial preparations and provide novel evidence that altered sympathetic responsiveness in the diabetic heart is partially dependent on alterations within the SAN itself.

4.5 Study limitations

This present study demonstrates the presence of impaired autonomic responsiveness of the SAN in diabetes using both *in vivo* and *ex vivo* measures. While these studies are of obvious importance, some limitations of our study should be noted. *In vivo* studies are absolutely necessary to the investigation of physiological processes as they allow us to test hypotheses in a live model, making the study more applicable to human models. However, they do not allow us to directly identify the underlying signaling pathways that mediate the physiological effects. Thus we will use data from isolated heart preparations and future work in isolated SAN myocytes to determine the cellular mechanism and pathways that may underlie our *in vivo* observations. Additionally, heart rates were recorded in mice anesthetized with isoflurane. While stable heart rates have previously been observed in mice anesthetized with isoflurane (Szczesny *et al.* 2004; Constantinides *et al.* 2011) we cannot exclude the possibility that isoflurane inhalation caused alterations in cardiac and metabolic function that may influence our results. We measured blood glucose in our T1D and T2D models and found that both groups of diabetic mice showed profoundly elevated blood glucose levels. However we

must note that our wildtype measurements of blood glucose from both the Akita group and the db/db group are different. This is likely due to the fact that blood glucose measurements were collected as random measures, meaning they are not fasting glucose levels. Therefore the difference seen in wildtype measurements is likely due to the difference in the time of day the measurements were taken or whether mice had recently eaten as food was given *ad libitum*. These differences could be further explored by taking fasting glucose measurements in future experiments.

In relation to our optical mapping work, we have used di-4-ANEPPS to measure changes in voltage. di-4-ANEPPS can have some direct transient effects on the heart (Fedorov *et al.* 2006); however, it is widely used for the kinds of applications used in our study (Herron *et al.* 2012). We also used Blebbistatin to suppress motion, to accurately assess the data without motion artifacts. Studies have demonstrated that blebbistatin is highly effective at preventing contraction without disrupting ion channels, action potential morphology or activation patterns (Fedorov *et al.* 2007; Lou *et al.* 2012; Azer *et al.* 2014). As previously mentioned our local CV measurements were produced using a previously established method (Morley *et al.* 1999; Nygren *et al.* 2004; Azer *et al.* 2014). Recent studies, however, have demonstrated that CV in the SAN is heterogeneous and anisotropic (Fedorov *et al.* 2006; Fedorov *et al.* 2012). Our measurements do not account for the anisotropic nature of CV in the SAN. Nevertheless, our method very effectively enables assessment of changes in local CV before and after application of pharmacological compounds. It is also well known that the SAN is an extremely heterogeneous region therefore it is possible that our measures of local CV from the activation site may incorporate multiple cell borders. However, our recorded CV data are

consistent with previous studies that report a relatively slow CV in the SAN (10 cm/sec or less) (Bleeker *et al.* 1980; Verheijck *et al.* 2001; Fedorov *et al.* 2006).

Lastly, this study utilized transgenic mice to model T1D and T2D. It is known that the use of both the Akita and the db/db mouse to model T1D and T2D are not a completely accurate representation of the disease in humans (Chatzigeorgiou *et al.* 2011; King *et al.* 2012). ß cell destruction in T1D is largely the result of an autoimmune response thus the Akita mutation may not fully account for all the pathological components of disease development (Yang and Santamaria, 2006). Similarly, the db/db mouse develops insulin resistant diabetes mellitus as a result of a monogenic mutation, which is rarely the case in humans with type 2 diabetes (King *et al.* 2012). Regardless of these issues both models have been used to investigate complications in diabetes in several studies, and are still considered to be accurate predictors of disease progression (Mathews *et al.*, 2002; Yoshida *et al.*, 2010; Drel *et al.*, 2011; Gault *et al.*, 2011; Park *et al.*, 2011; Zhou *et al.*, 2011).

4.6 Future directions

Diabetes is a highly complex disease that may alter cardiac function via a number of mechanisms. These may include glucose toxicity, the generation of reactive oxygen species, metabolic disorders, and alterations in insulin-dependent signaling pathways (Bugger and Abel, 2010; Luo *et al.* 2013). Thus current and future work will aim to understand possible molecular mechanisms in for impaired autonomic responsiveness in the SAN. Some of our current isolated cell work implicates insulin-dependent PI3K signaling in the parasympathetic dysfunction seen in the SAN in the diabetic heart in the

Akita model. Therefore, further *in vivo* and molecular studies will also be necessary to characterize the altered sympathetic responsiveness demonstrated in our optical mapping data and understand possible mechanistic targets. These findings will provide a framework for future studies to identify potential targets for intervention in diabetic patients. While the main focus of our study was on parasympathetic regulation of the SAN in diabetes our study also clearly shows that there are baseline reductions in HR and SAN function in Akita mice. This is consistent with a prior study using a streptozotocin-induced model of T1D, which also showed baseline reductions in HR and cSNRT compared to normal mice. These baseline differences were attributed to apoptosis of SAN myocytes due to enhanced levels of oxidized Ca^{2+}/calmodulin dependent protein kinase II (Luo et al. 2013).

4.7 Conclusions

T1D and T2D are highly prevalent metabolic disorders that are frequently associated with fatal cardiovascular complications. CAN is a severe cardiovascular complication in diabetes and results in progressive decline of proper autonomic regulation of heart rate. The etiology of CAN is largely unknown, but it is recognized as a significant contributor to mortality in diabetes. CAN is associated with impaired parasympathetic and sympathetic responsiveness of the heart and was originally thought to be solely a consequence of nerve damage. Recent work has implicated defects within the heart itself as a major player in autonomic dysfunction in diabetes. Based on this premise, we aimed to investigate the presence of altered autonomic responsiveness of the SAN in diabetes. In summary, the present findings demonstrate that the Akita and db/db mouse model of diabetes recapitulate the impaired parasympathetic regulation of the

heart associated with diabetes and that the impaired effects can be rescued by insulin treatment. They also demonstrate that the Akita mouse also models possible sympathetic impairments reported in diabetic patients. Taken together these novel results implicate intrinsic alterations in SAN function as a target of impaired autonomic responsiveness in diabetes.

REFERENCES

Atkinson MA, Maclaren NK.The pathogenesis of insulin-dependent diabetes mellitus. *N Engl J Med.* 1994 Nov 24;331(21):1428-36

Azer J, Hua R, Krishnaswamy PS, Rose RA. Effects of natriuretic peptides on electrical conduction in the sinoatrial node and atrial myocardium of the heart. *J Physiol*. 2014;592:1025-1045

Banthia S1, Bergner DW, Chicos AB, Ng J, Pelchovitz DJ, Subacius H, Kadish AH, Goldberger JJ. Detection of cardiovascular autonomic neuropathy using exercise testing in patients with type 2 diabetes mellitus. *J Diabetes Complications*. 2013 Jan-Feb;27(1):64-9

Belke DD1, Severson DL.Diabetes in mice with monogenic obesity: the db/db mouse and its use in the study of cardiac consequences. *Methods Mol Biol.* 2012;933:47-57.

Bleeker WK, Mackaay AJ, Masson-Pevet M, Bouman LN, Becker AE. Functional and morphological organization of the rabbit sinus node. *Circ Res*. 1980;46:11-22

Bouman LN, Gerlings ED, Biersteker PA & Bonke FI (1968). Pacemaker shift in the sino-atrial node during vagal stimulation. *Pflugers Arch* 302, 255–267.

Boineau JP, Schuessler RB, Mooney CR, Wylds AC, Miller CB, Hudson RD, Borremans JM, Brockus CW. Multicentric origin of the atrial depolarization wave: the pacemaker complex. Relation to dynamics of atrial conduction, P-wave changes and heart rate control. *Circulation*. 1978;58:1036 –1048.

Boineau JP, Canavan TE, Schuessler RB, Cain ME, Corr PB, Cox JL. Demonstration of a widely distributed atrial pacemaker complex in the human heart. *Circulation* 77: 1221–1237, 1988.

Boyett MR, Honjo H, Kodama I. The sinoatrial node, a heterogeneous pacemaker structure. *Cardiovasc Res* 47: 658–687, 2000.

Boyett MR, Honjo H, Yamamoto M, Nikmaram MR, Niwa R, Kodama I. Downward gradient in action potential duration along conduction path in and around the sinoatrial node. *Am J Physiol*. 1999;276:H686 –H698.

Bugger H, Abel ED. Mitochondria in the diabetic heart. *Cardiovasc Res*. 2010;88:229-240

Bugger H, Boudina S, Hu XX, Tuinei J, Zaha VG, Theobald HA, Yun UJ, McQueen AP, Wayment B, Litwin SE, Abel ED. Type 1 diabetic akita mouse hearts are insulin sensitive but manifest structurally abnormal mitochondria that remain coupled despite increased uncoupling protein 3. *Diabetes*. 2008;57:2924-2932

Chadda KD, Banka VS, Bodenheimer MM, Helfant RH. Corrected sinus node recovery time. Experimental physiologic and pathologic determinants. *Circulation*. 1975;51:797-801

Chatzigeorgiou A1, Halapas A, Kalafatakis K, Kamper E. The use of animal models in the study of diabetes mellitus. *in vivo.* 2009 Mar-Apr;23(2):245-58.

Chen H, Charlat O, Tartaglia LA, Woolf EA, Weng X, Ellis SJ, Lakey ND, Culpepper J, Moore KJ; Breitbart RE; Duyk GM; Tepper RI; Morgenstern JP. Evidence that the diabetes gene encodes the leptin receptor: identification of a mutation in the leptin receptor gene in db/db mice. *Cell* 1996. 84(3):491-5.

Coppen SR, Kodama I, Boyett MR *et al.* Connexin 45, a major connexin of the rabbit sinoatrial node, is co-expressed with connexin43 in a restricted zone at the nodal-crista terminalis border. J Histochem Cytochem 1999;47:907–918.

Danaei G, Finucane MM, Lu Y, Singh GM, Cowan MJ, Paciorek CJ *et al.* National, regional, and global trends in fasting plasma glucose and diabetes prevalence since 1980: systematic analysis of health examination surveys and epidemiological studies with 370 country-years and 2.7 million participants. *Lancet*, 2011, 378(9785):31–40.

Constantinides C, Mean R, Janssen BJ. Effects of isoflurane anesthesia on the cardiovascular function of the C57BL/6 mouse. *ILAR J* 2011;52:E21-E31.

Davies LM, Kanter HL, Beyer EC, Saffitz JE. Distinct gap junction protein phenotypes in cardiac tissues with disparate conduction properties. J Am Coll Cardiol 1994;24:1124–1132.

Davis TM, Parsons RW, Broadhurst RJ, Hobbs MS, Jamrozik K. Arrhythmias and mortality after myocardial infarction in diabetic patients. Relationship to diabetes treatment. *Diabetes Care*. 1998 Apr;21(4):637-40

DiFrancesco D. Pacemaker mechanisms in cardiac tissue. *Annu Rev Physiol*. 1993;55:455-472

Dinçer UD1, Bidasee KR, Güner S, Tay A, Ozçelikay AT, Altan VM. The effect of diabetes on expression of beta1-, beta2-, and beta3-adrenoreceptors in rat hearts. *Diabetes*. 2001 Feb;50(2):455-61.

Dobrzynski H, Boyett MR, Anderson RH. New insights into pacemaker activity: promoting understanding of sick sinus syndrome. *Circulation*. 2007;115:1921-1932.

Drel VR, Pacher P, Stavniichuk R, Xu W, Zhang J, Kuchmerovska TM *et al.* (2011). Poly(ADP-ribose)polymerase inhibition counteracts renal hypertrophy and multiple manifestations of peripheral neuropathy in diabetic Akita mice. Int J Mol Med 28: 629–635.

Eaton RP, Berman M, Steinberg D. Kinetic studies of plasma free fatty acid and triglyceride metabolism in man. *J Clin Invest* 1969; 48: 1560-79

Efimov IR, Fahy GJ, Cheng YN, Van Wagoner DR, Tchou PJ, Mazgalev TN. High-resolution fluorescent imaging of rabbit heart does not reveal a distinct atrioventricular nodal anterior input channel (fast pathway) during sinus rhythm. *J Cardiovasc Electrophysiol*. 1997;8: 295–306.

Efimov IR, Fedorov VV, Joung B, Lin SF. Mapping cardiac pacemaker circuits: methodological puzzles of the sinoatrial node optical mapping. *Circ Res*. 2010 Feb 5;106(2):255-71

Efimov IR, Nikolski VP & Salama G (2004). Optical imaging of the heart. *Circ Res* 95, 21–33.

Eyster JAE, Meek WJ. Experiments on the origin and propagation of the impulse in the heart: point of primary negativity in the mammalian heart and the spread of negativity to other regions. *Heart*. 1913;5:119–136.

Elvan A, Wylie K, Zipes DP. Pacing-induced chronic atrial fibrillation impairs sinus node function in dogs. Electrophysiological remodeling. *Circulation*. 1996 Dec 1;94(11):2953-60.

en Velde I, de Jonge B, Verheijck EE *et al.* Spatial distribution of connexin43, the major cardiac gap junction protein, visualizes the cellular network for impulse propagation from sinoatrial node to atrium. Circ Res 1995;76:802–811.

Ewing DJ, Clarke BF. Diagnosis and management of diabetic autonomic neuropathy. *Br Med J (Clin Res Ed)*. 1982 Oct 2;285(6346):916-8

Fajans, S.S. 1990. Scope and heterogeneous nature of MODY. *Diabetes Care.* 13:49–64.

Fazan R Jr, Ballejo G, Salgado MC, Moraes MF, Salgado HC. Heart rate variability and baroreceptor function in chronic diabetic rats. *Hypertension.* 1997 Sep;30(3 Pt 2):632-5.

Fedorov VV, Chang R, Glukhov AV, Kostecki G, Janks D, Schuessler RB, Efimov IR. Complex interactions between the sinoatrial node and atrium during reentrant arrhythmias in the canine heart. *Circulation*. 2010;122:782-789

Fedorov VV, Glukhov AV & Chang R (2012). Conduction barriers and pathways of the sinoatrial pacemaker complex: their role in normal rhythm and atrial arrhythmias. *Am J Physiol Heart Circ Physiol* 302, H1773–1783.

Fedorov VV, Glukhov AV, Chang R, Kostecki G, Aferol H, Hucker WJ, Wuskell JP, Loew LM, Schuessler RB, Moazami N, Efimov IR.Optical mapping of the isolated coronary-perfused human sinus node. J Am Coll Cardiol. 2010 Oct 19;56(17):1386-94

Fedorov VV, Hucker WJ, Dobrzynski H, Rosenshtraukh LV, Efimov IR. Postganglionic nerve stimulation induces temporal inhibition of excitability in rabbit sinoatrial node. *Am J Physiol Heart Circ Physiol*. 2006;291:H612-623

Fedorov VV, Lozinsky IT, Sosunov EA, Anyukhovsky EP, Rosen MR, Balke CW & Efimov IR (2007). Application of blebbistatin as an excitation–contraction uncoupler for electrophysiologic study of rat and rabbit hearts. *Heart Rhythm* 4, 619–626.

Fedorov VV, Schuessler RB, Hemphill M, Ambrosi CM, Chang R, Voloshina AS, Brown K, Hucker WJ, Efimov IR. Structural and functional evidence for discrete exit pathways that connect the canine sinoatrial node and atria. *Circ Res*. 2009;104:915-923

Fujita H1, Haseyama T, Kayo T, Nozaki J, Wada Y, Ito S, Koizumi A. Increased expression of glutathione S-transferase in renal proximal tubules in the early stages of diabetes: a study of type-2 diabetes in the Akita mouse model. *Exp Nephrol.* 2001;9(6):380-6.

Gan MJ, Albanese-O'Neill A, Haller MJ. Type 1 diabetes: current concepts in epidemiology, pathophysiology, clinical care, and research. *Curr Probl Pediatr Adolesc Health Care*. 2012 Nov-Dec;42(10):269-91

Garris DR. 2004. Ultrastructural analysis of progressive endometrial hypercytolipidemia induced by obese (ob/ob) and diabetes (db/db) genotype mutations: structural basis of female reproductive tract involution. *Tissue Cell* 36(1):19-28.

Garris DR; Garris BL. 2003. Diabetes (db/db) mutation-induced ovarian involution: progressive hypercytolipidemia. *Exp Biol Med (Maywood*) 228(9):1040-50.

Gault VA, Kerr BD, Harriott P, Flatt PR (2011). Administration of an acylated GLP-1 and GIP preparation provides added beneficial glucose-lowering and insulinotropic actions over single incretins in mice with Type 2 diabetes and obesity. Clin Sci (Lond) 121: 107–117.

Greer JJ; Ware DP; Lefer DJ. 2006. Myocardial infarction and heart failure in the db/db diabetic mouse. *Am J Physiol Heart Circ Physiol* 290(1):H146-53.

Gehrmann J, Meister M, Maguire CT, Martins DC, Hammer PE, Neer EJ, Berul CI, Mende U. Impaired parasympathetic heart rate control in mice with a reduction of functional g protein betagamma-subunits. *Am J Physiol Heart Circ Physiol*. 2002;282:H445-456

Glukhov AV, Fedorov VV, Anderson ME, Mohler PJ, Efimov IR. Functional anatomy of the murine sinus node: High-resolution optical mapping of ankyrin-b heterozygous mice. *Am J Physiol Heart Circ Physiol*. 2010;299:H482-491

Gomes JA, Hariman RI, Chowdry IA. New application of direct sinus node recordings in man: assessment of sinus node recovery time. *Circulation.* 1984;70(4):663–671.

Goncalves AC1, Tank J, Diedrich A, Hilzendeger A, Plehm R, Bader M, Luft FC, Jordan J, Gross V.Diabetic hypertensive leptin receptor-deficient db/db mice develop cardioregulatory autonomic dysfunction. *Hypertension*. 2009 Feb;53(2):387-92

Hall S. and A. Cooke, Autoimmunity and inflammation: murine models and translational studies, *Mammalian Genome*, vol. 22, no. 7-8, pp. 377–389, 2011.
Herron TJ, Lee P & Jalife J (2012). Optical imaging of voltage and calcium in cardiac cells & tissues. *Circ Res* 110, 609–623

Hsueh W, Abel ED, Breslow JL, Maeda N, Davis RC, Fisher EA, Dansky H, McClain DA, McIndoe R, Wassef MK, Rabadan-Diehl C, Goldberg IJ. Recipes for creating animal models of diabetic cardiovascular disease. *Circ Res*. 2007;100:1415-1427

Hummel KP; Dickie MM; Coleman DL. 1966. Diabetes, a new mutation in the mouse. *Scienc*e 153(740):1127-8.

Irisawa H, Brown HF, Giles W. Cardiac pacemaking in the sinoatrial node. *Physiol Rev*. 1993;73:197-227

Izumi T, Yokota-Hashimoto H, Zhao S, Wang J, Halban PA, Takeuchi T. Dominant negative pathogenesis by mutant proinsulin in the Akita diabetic mouse. *Diabetes.* 2003;52:409–416.

Javorka M1, Javorkova J, Tonhajzerova I, Javorka K. Parasympathetic versus sympathetic control of the cardiovascular system in young patients with type 1 diabetes mellitus. *Clin Physiol Funct Imaging*. 2005 Sep;25(5):270-4.

Joyner RW, van Capelle FJL. Propagation through electrically coupled cells: how a small SA node drives a large atrium. *Biophys J* 1986;50:1157–1164.

Kahn JK, Sisson JC, Vinik AI. Prediction of sudden cardiac death in diabetic autonomic neuropathy. *J Nucl Med*. 1988;29:1605–1606.

Kayo T, Koizumi A. Mapping of murine diabetogenic gene mody on chromosome 7 at D7Mit258 and its involvement in pancreatic islet and beta cell development during the perinatal period. *J Clin Invest*. 1998;101:2112-2118.

Kodama I, Boyett MR, Suzuki R, Honjo H & Toyama J (1996). Regional differences in the response of the isolated sino-atrial node of the rabbit to vagal stimulation. *J Physiol* 495, 785–801.

King AJ. The use of animal models in diabetes research.*Br J Pharmacol*. 2012 Jun;166(3):877-94

Lakatta EG, Maltsev VA, Vinogradova TM. A coupled system of intracellular ca2+ clocks and surface membrane voltage clocks controls the timekeeping mechanism of the heart's pacemaker. *Circ Res*. 2010;106:659-673

Lee JH, Yang SH, Oh JM, Lee MG. Pharmacokinetics of drugs in rats with diabetes mellitus induced by alloxan or streptozocin: comparison with those in patients with type I diabetes mellitus. *J Pharm Pharmacol* 2010. 62: 1–23.

Lou Q, Li W & Efimov IR (2012). The role of dynamic instability and wavelength in arrhythmia maintenance as revealed by panoramic imaging with blebbistatin vs. 2,3-butanedione monoxime. *Am J Physiol Heart Circ Physiol* 302, H262–H269.

Liu J, Dobrzynski H, Yanni J, Boyett MR, Lei M. Organisation of the mouse sinoatrial node: Structure and expression of hcn channels. *Cardiovasc Res*. 2007;73:729-738

Lu Z, Jiang YP, Xu XH, Ballou LM, Cohen IS, Lin RZ .Decreased L-type Ca2+ current in cardiac myocytes of type 1 diabetic Akita mice due to reduced phosphatidylinositol 3-kinase signaling. *Diabetes*. 2007 Nov;56(11):2780-9.

Luo M, Guan X, Luczak ED, Lang D, Kutschke W, Gao Z, Yang J, Glynn P, Sossalla S, Swaminathan PD, Weiss RM, Yang B, Rokita AG, Maier LS, Efimov IR, Hund TJ, Anderson ME. Diabetes increases mortality after myocardial infarction by oxidizing camkii. *J Clin Invest*. 2013;123:1262-1274

McDowell TS, Hajduczok G, Abboud FM, Chapleau MW. Baroreflex dysfunction in diabetes mellitus. II. Site of baroreflex impairment in diabetic rabbits. *Am J Physiol.* 1994 Jan;266(1 Pt 2):H244-9.

Mackaay AJ, Op't Hof T, Bleeker WK, Jongsma HJ & Bouman LN (1980). Interaction of adrenaline and acetylcholine on cardiac pacemaker function. Functional inhomogeneity of the rabbit sinus node. *J Pharmacol Exp Ther* 214, 417–422.

Mangoni ME, Nargeot J. Properties of the hyperpolarization-activated current (i(f)) in isolated mouse sino-atrial cells. *Cardiovasc Res*. 2001;52:51-64

Maser RE, Mitchell BD, Vinik AI, Freeman R. The association between cardiovascular autonomic neuropathy and mortality in individuals with diabetes: a meta-analysis. *Diabetes Care*. 2003;26:1895-1901.

Mathews CE, Langley SH, Leiter EH (2002). New mouse model to study islet transplantation in insulin-dependent diabetes mellitus. *Transplantation* 73: 1333–1336.

Meek WJ, Eyster JAE. The effect of vagal stimulation and of colling on the location of the pacemaker within the sino-auricular node. *Am J Physiol*. 1914;34:368 –383.

Mighiu AS, Heximer SP. Controlling Parasympathetic Regulation of Heart Rate: A Gatekeeper Role for RGS Proteins in the Sinoatrial Node. *Front Physiol*. 2012 Jun 13;3:204

Morley GE, Vaidya D, Samie FH, Lo C, Delmar M, Jalife J. Characterization of conduction in the ventricles of normal and heterozygous cx43 knockout mice using optical mapping. *J Cardiovasc Electrophysiol*. 1999;10:1361-1375

Nalos PC, Deng Z, Rosenthal ME, Gang ES, Oseran DS, Mandel WJ, Peter T. Hemodynamic influences on sinus node recovery time: effects of autonomic blockade. *J Am Coll Cardiol*. 1986 May;7(5):1079-86.

Narula OS, Samet P, Javier RP. Significance of the sinus-node recovery time. *Circulation*. 1972;45:140-158

Nygren A, Lomax AE & Giles WR (2004). Heterogeneity of action potential durations in isolated mouse left and right atria recorded using voltage-sensitive dye mapping. *Am J Physiol Heart Circ Physiol* 287, H2634–H2643.

Oosthoek PW, Viragh S, Mayen AEM *et al.* Immunohistochemical delineation of the conduction system. I: the sinoatrial node. Circ Res 1993;73:473 – 481.

Ong JM, Kern PA. Effect of feeding and obesity on lipoprotein lipase activity, immunoreacrive protein and messenger RNA levels in human adipose tissue. *J Clin Invest* 1989; 84: 305-11

Oyadomari S, Koizumi A, Takeda K, *et al.* Targeted disruption of the Chop gene delays endoplasmic reticulum stress-mediated diabetes. *J Clin Invest*. 2002;109:525–532.

Oudit GY, Sun H, Kerfant BG, Crackower MA, Penninger JM, Backx PH. The role of phosphoinositide-3 kinase and pten in cardiovascular physiology and disease. *J Mol Cell Cardiol*. 2004;37:449-471

Park JS, Rhee SD, Kang NS, Jung WH, Kim HY, Kim JH *et al.* (2011). Anti-diabetic and anti-adipogenic effects of a novel selective 11beta-hydroxysteroid dehydrogenase type 1 inhibitor, 2-(3-benzoyl)-4-hydroxy-1,1-dioxo-2H-1,2-benzothiazine-2-yl-1- phenylethano ne (KR-66344). Biochem Pharmacol 81:1028–1035.

Park HJ, Zhang Y, Du C, Welzig CM, Madias C, Aronovitz MJ, Georgescu SP, Naggar I, Wang B, Kim YB, Blaustein RO, Karas RH, Liao R, Mathews CE, Galper JB. Role of SREBP-1 in the development of parasympathetic dysfunction in the hearts of type 1 diabetic Akita mice. *Circ Res*. 2009;105:287-294.

Perciaccante A1, Fiorentini A, Paris A, Serra P, Tubani L. Circadian rhythm of the autonomic nervous system in insulin resistant subjects with normoglycemia, impaired fasting glycemia, impaired glucose tolerance, type 2 diabetes mellitus. *BMC Cardiovasc Disord*. 2006 May 2;6:19.

Pickup J, Keen H. Continuous subcutaneous insulin infusion at 25 years: evidence base for the expanding use of insulin pump therapy in type 1 diabetes. *Diabetes Care*. 2002 Mar;25(3):593-8

Pop-Busui R, Low PA, Waberski BH, Martin CL, Albers JW, Feldman EL, Sommer C, Cleary PA, Lachin JM, Herman WH. Effects of prior intensive insulin therapy on cardiac autonomic nervous system function in type 1 diabetes mellitus: the Diabetes Control and Complications Trial/Epidemiology of Diabetes Interventions and Complications study (DCCT/ EDIC). *Circulation* 2009; 119: 2886-2893

Robinson B, Epstein S, Beiser G.D, Braunwald E. Control of Heart Rate by the Autonomic Nervous System: Studies in Man on the Interrelation Between Baroreceptor Mechanisms and Exercise *Circulation Research* 1966; 19: 400-411

Russell JW, Sullivan KA, Windebank AJ, Herrmann DN, Feldman EL.
Neurons undergo apoptosis in animal and cell culture models of diabetes. *Neurobiol Dis*. 1999;6:347–363.

Sano T, Yamagishi S. Spread of excitation from the sinus node. *Circ Res*. 1965;16:423–430.

Schreihofer AM, Mandel DA, Mobley SC, Stepp DW. Impairment of sympathetic baroreceptor reflexes in obese Zucker rats. *Am J Physiol Heart Circ Physiol.* 2007;293:H2543–2549.

Schuessler RB. Abnormal sinus node function in clinical arrhythmias. *J Cardiovasc Electrophysiol*. 2003;14:215–217.

Szczesny G, Veihelmann A, Massberg S, Nolte D, Messmer K. Long-term anaesthesia using inhalatory isoflurane in different strains of mice-the haemodynamic effects. *Lab Anim.* 2004;38:64-69.

Severs NJ. The cardiac gap junctions and intercalated disc. *Int J Cardiol* 1990;26:137 – 173.

Shaw JE, Sicree RA, Zimmet PZ.Global estimates of the prevalence of diabetes for 2010 and 2030. *Diabetes Res Clin Pract*. 2010 Jan;87(1):4-14.

Shibata N, Inada S, Mitsui K, Honjo H, Yamamoto M, Niwa R, Boyett MR, Kodama I. Pacemaker shift in the rabbit sinoatrial node in response to vagal nerve stimulation. *Exp Physiol* 86: 177–184, 2001.

Stevens M, Dayanikli F, Raffel D, Allman K, Standford T, Feldman E, Wieland D, Corbett J, Schwaiger M. Scintigraphic assessment of regionalized defects in myocardial sympathetic intervation and blood flow regulation in diabetic patients with autonomic neuropathy. *J Am Coll Cardiol*. 1988;31:1575–1584.

Suarez GA, Clark VM, Norell JE, Kottke TE, Callahan MJ, O'Brien PC, Low PA, Dyck PJ. Sudden cardiac death in diabetes mellitus: risk factors in the Rochester Diabetic Neuropathy Study. *J Neurol Neurosurg Psy- chiatry*. 2005;76:240–245.

Swoap SJ, Li C, Wess J, Parsons AD, Williams TD, Overton JM. Vagal tone dominates autonomic control of mouse heart rate at thermoneutrality. *Am J Physiol Heart Circ Physiol.* 2008 ;294(4):1581-8

Thayer, T.C, Wilson S.B., Mathews C.E, Use of nonobese diabetic mice to understand human type 1 diabetes," *Endocrinol- ogy and Metabolism Clinics of North America*, vol. 39, no. 3, pp. 541–561, 2010.

Thomas SP, Kucera JP, Bircher-Lehmann L, Rudy Y, Saffitz JE, Kléber AG. Impulse propagation in synthetic strands of neonatal cardiac myocytes with genetically reduced levels of connexin 43.*Circ Res*. 2003 Jun 13;92(11):1209-16.

The effect of intensive diabetes therapy on measures of auto- nomic nervous system function in the Diabetes Control and Complications Trial (DCCT). *Diabetologia* 1998

Tonkin AM, Tornos P, Heddle WF, Rapp H. Autonomic effects on the human cardiac conduction system. Evaluation by intracardiac electrocardiography and programmed stimulation techniques. *Br Heart J.* 1980 Aug;44(2):168-74

Van Buren T, Schiereck P, De Ruiter GJ, Gispen WH, De Wildt DJ.Vagal efferent control of electrical properties of the heart in experimental diabetes. *Acta Diabetol*. 1998 Apr;35(1):19-25.

van Kempen MJA, Fromaget C, Gross D, Moorman AFM, Lamers WH. Spatial distribution of connexin43, the major gap junction protein in the developing and adult rat heart. *Circ Res* 1991;68:1638 – 1651.

Veenstra RD, Wang H-Z, Beblo DA *et al.* Selectivity of connexin- specific gap junctions does not correlate with channel conductance. *Circ Res* 1995;77:1156–1165.

Veenstra RD, Wang H-Z, Westphale EM, Beyer EC. Multiple connexins confer distinct regulatory and conductance properties of gap junctions in developing heart. *Circ Res* 1992;71:1277 – 1283

Verheule S. Distribution and physiology of mammalian cardiac gap junctions. Dissertation, University of Utrecht, 1999.

Verheijck EE, van Kempen MJ, Veereschild M, Lurvink J, Jongsma HJ, Bouman LN. Electrophysiological features of the mouse sinoatrial node in relation to connexin distribution. *Cardiovasc Res*. 2001;52:40-50

Vinik AI, Ziegler D. Diabetic cardiovascular autonomic neuropathy. *Circulation*. 2007;115:387-397.

Vinogradova TM, Fedorov VV, Yuzyuk TN, Zaitsev AV & Rosenshtraukh LV (1998). Local cholinergic suppression of pacemaker activity in the rabbit sinoatrial node. *J Cardiovasc Pharmacol* 32, 413–424.

Wang J, Takeuchi T, Tanaka S, *et al.* A mutation in the insulin 2 gene induces diabetes with severe pancreatic beta-cell dysfunction in the Mody mouse. *J Clin Invest*. 1999;103:27–37.

Wahrenberg H, Lonnqvist F, Arner P. Mechanisms underlying regional differences in lipolysis in human adipose tissue. *Clin Invest* 1989; 84: 458-6

Whiting DR, Guariguata L, Weil C, Shaw J. IDF diabetes atlas: global estimates of the prevalence of diabetes for 2011 and 2030. *Diabetes Res Clin Pract*. 2011 Dec;94(3):311-21.

Wild S, Roglic G, Green A, Sicree R, King H. Global prevalence of diabetes: estimates for the year 2000 and projections for 2030. *Diabetes Care*. 2004;27:1047-1053.

Yang Y, Santamaria P (2006). Lessons on autoimmune diabetes from animal models. Clin Sci (Lond) 110: 627–639.

Yoon JW, Jun HS. Autoimmune destruction of pancreatic beta cells. *Am J Ther*. 2005 Nov-Dec;12(6):580-91.

Yoshida S, Tanaka H, Oshima H, Yamazaki T, Yonetoku Y, Ohishi T *et al.* (2010). AS1907417, a novel GPR119 agonist, as an insulinotropic and beta-cell preservative agent for the treatment of type 2 diabetes. *Biochem Biophys Res Commun* 400: 745–751.

Zhang Y, Welzig CM, Picard KL, Du C, Wang B, Pan JQ, Kyriakis JM, Aronovitz MJ, Claycomb WC, Blanton RM, Park HJ, Galper JB. Glycogen synthase kinase-3beta inhibition ameliorates cardiac parasympathetic dysfunction in type 1 diabetic akita mice. *Diabetes*. 2014;63:2097-2113

Zhou C, Pridgen B, King N, Xu J, Breslow JL (2011). Hyperglycemic Ins2AkitaLdlr-/- mice show severely elevated lipid levels and increased atherosclerosis: a model of type 1 diabetic macrovascular disease. *J Lipid Res* 52: 1483–1493.

Zimmet P, Alberti KG, Shaw J. Global and societal implications of the diabetes epidemic. *Nature*. 2001;414:782-787